Advanced Journal of Chemistry, Section A, 2024, 7(5), 576-606

Advanced Journal of Chemistry, Section A

journal homepage: www.ajchem-a.com

Original Research Article

In Depth Computational Screening of Novel Indane-1, 3-Dione Derivatives as Potential Anti-Tubercular Agents

Nitin Arjun Londhe [1,*], Karthickeyan Krishnan [2]

[1]*School of Pharmaceutical Sciences, Vels Institute of Science, Technology and Advanced Studies (VISTAS), Pallavaram, Chennai, Tamil Nadu, 600117, India*
[2]*Department of Pharmacy Practice, School of Pharmaceutical Sciences, Vels Institute of Science, Technology and Advanced Studies (VISTAS), Pallavaram, Chennai, Tamil Nadu, 600117, India*

ARTICLEINFO

Article history

Submitted: 22 March 2024
Revised: 16 May 2024
Accepted: 28 May 2024

Manuscript ID: AJCA-2404-1514
Checked for Plagiarism: Yes
Language Editor Checked: Yes
DOI: **10.48309/AJCA.2024.453614.1514**

KEYWORDS

Indane 1,3 dione
Molecular docking
Molecular dynamics
In silico ADMET

ABSTRACT

Mycobacterium TB poses a significant challenge by developing resistance to currently available medications, making it a serious global health concern. Therefore, it is imperative to create novel medications that exhibit efficacy against diverse strains of Tuberculosis. Isoniazid (INH) is a primary anti-tubercular medication that works against Mycobacterium TB by blocking the activity of a specific enzyme called InhA, which is responsible for reducing a compound called 2-trans-enoyl-acyl carrier protein. The aim of this study was to pinpoint novel inhibitors of the enoyl-acyl carrier protein (ACP) reductase InhA. This work specifically examines the use of in silico techniques molecular docking and molecular dynamic simulation to study designed substituted Indane-1, 3-dione derivatives (1-15). The *In silico* ADMET screening was conducted using the SwissADME and admet SAR online ADME prediction tool server and passes Lipinski's rule of five as well as pharmacokinetic features like skin permeability and molar refractivity lies with in limit which shows none of noticeable signs of toxicity. The stability of the docked complex was assessed by conducting a Molecular Dynamics (MD) simulation using Schrodinger Desmond over 100 ns. Most of the residues in the root mean square fluctuation (RMSF) fell between the range of 0.5-4 Å and radius of gyration ranges between 18.1 to 18.4 Å throughout the 100 ns simulation reflects maintaining stability of protein complex during the catalytic activity. Most of compounds shows higher GI absorption and inhibits CYP-3A4, CYP-2D6, CYP promiscuity shows range from 0.5-0.9. Compound 11 have highest docking score of -10.38 kcal/mol and shows excellent hydrophobic and hydrophilic interactions with most of amino acid residues. Moreover, compound 11 were found to be safe for acute inhalation and cutaneous sensitization. Thus, the obtained results suggest that compound 11, 2-[(trifluoromethyl) phenyl] methylidene-1*H*-indene-1, 3-(2*H*)-dione appear to be good candidates for drugs with a potential leading structure for further development.

* Corresponding author: Londhe, Nitin Arjun
✉ E-mail: nit.londhe@gmail.com

GRAPHICAL ABSTRACT

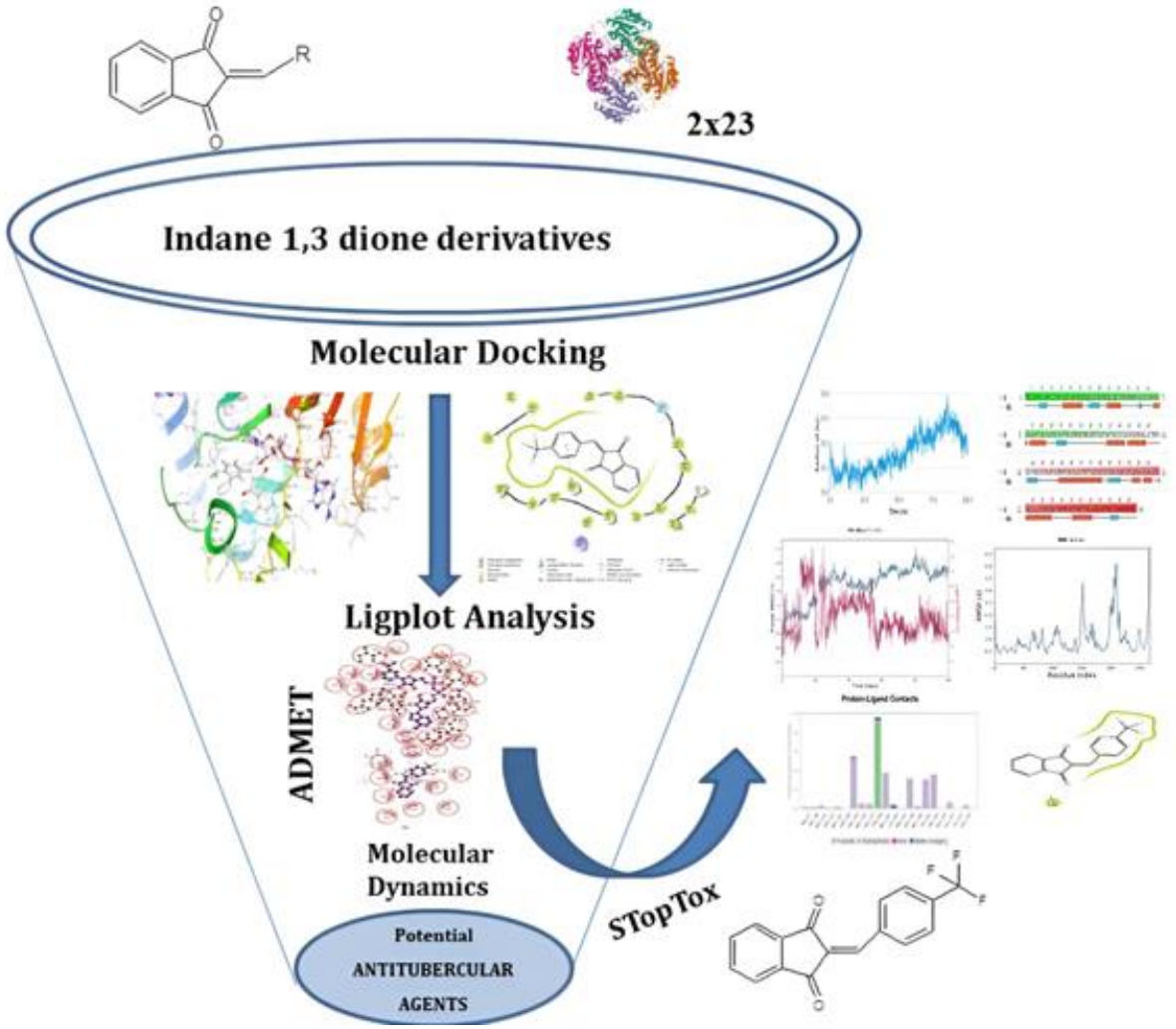

Introduction

Tuberculosis (TB) a contagious airborne disease caused by Mycobacterium tuberculosis (Mtb) bacteria [1]. Following the COVID-19 pandemic, tuberculosis (TB) became the most common infectious agent-related cause of death, surpassing HIV/AIDS. When deaths are included in, it comes in at number 13 in the world with about 1.5 million [2]. The quality of tuberculosis care offered internationally has been a top issue for various nations after the SARS-CoV outbreak [3]. The synergistic effects of co-infection with both SARS-CoV-2 and TB, namely via TB programming, on prognoses remain unclear [3-4]. There were 7.5 million newly diagnosed TB cases globally in 2022, according to official reports [5].

Tubercular Mycobacteria are acid-fast bacilli categorised as gram-positive. People who have tuberculosis cough out germs into the air, which is how the disease is often transmitted. Although tuberculosis (TB) is thought to be present in around 25% of the world's population, the majority of those carriers do not get the disease [6-8]. There are others who will be able to overcome the sickness. Infections are diagnosed by a chest X-ray, microbacterial cultures, and a

tuberculin skin test [9]. Adults are affected by tuberculosis (TB) in around 90% of cases each year; males are affected more often than women [10]. The illness may affect other regions of the body, albeit its primary manifestation is pulmonary tuberculosis.

Antimicrobial drugs are needed to treat tuberculosis (TB); these drugs include aminoglycosides and fluoroquinolones as second-line treatments and isoniazid, rifampin, and pyrazinamide as first-line treatments [11].The development of medication resistance in different Mycobacterium strains is a significant barrier to the successful treatment of TB and will affect around 500,000 of the 6.4 million new cases of tuberculosis in 2021[12].

Fluoroquinolones, rifampin, and isoniazid are examples of anti-tubercular drugs that are resistant to the mycobacterium that causes pre-extensively drug-resistant tuberculosis (pre-XDR TB) [13].

A multitude of factors contribute to chemotherapy treatment failures, including the treatment's high degree of complexity (three or more medications may be used), its lengthy duration (six to nine months, or even up to 24 months), and its numerous side effects (epistaxis, nausea, vomiting, and dyspepsia, among others) as well as resistance against microbes [14-18].

The number of cases with extended drug-resistant (XDR) and multidrug-resistant (MDR) TB has increased, making treatment more challenging and expensive. Finding innovative treatment alternatives with a minimal risk of resistance is thus essential [19].

Mycobacterium TB and other closely related species' cell membranes are mostly composed of long-chain fatty acids known as mycolic acids [20]. Long chain fatty acid biosynthesis involves two types of fatty acid synthases (FASs): the multifunctional eukaryotic FAS I enzyme and the acyl carrier protein (ACP)-dependent FAS II systems. Each unique monofunctional protein that makes up the FAS II systems is responsible for catalysing a particular pathway reaction [21].

Enoyl-ACP reductase is a crucial part of the FAS-II system of Mycobacterium, which is in control of fatty acid synthesis. Owing to its dissimilarity in the human body, this enzyme may be a potential target for novel anti-tubercular drugs [22].

Mycobacterium TB InhA (enoyl-ACP reductase) is an enzyme involved in the tuberculosis bacterium's fatty acid production pathway. It is required for the manufacture of mycolic acids, which are structural components of the mycobacterial cell wall [23]. Mycolic acids give the cell wall structural stability, making it impervious to many antibiotics and helping the bacterium resist host defences. The key enzyme systems involved in synthesis of mycolic acids, which are essential components of the cell wall in Mycobacterium tuberculosis (M. tuberculosis), involves a complex enzymatic system which includes β-Ketoacyl-Acyl Carrier Protein Synthase (KAS) involved in chain elongation, Fatty Acid Synthase (FAS-I and FAS-II) involved in formation as well as elongation of long-chain fatty acids, Mycolyl-Transferase Complex have role in transfer of mycolic acids to form outer cellwall, Enoyl-Acyl Carrier Protein Reductase (InhA) involved in formation of saturated fatty acids by reducing trans-2-enoyl-ACP which is target for a number of antitubercular drugs, including isoniazid (INH). Therefore, InhA (enoyl-ACP reductase) is chosen for molecular docking investigations [24].

Previous studies have shown that 1, 3-indanedione derivatives exhibit a wide range of biological properties. These properties include antiviral, antibacterial, antifungal, anticancer, anti-inflammatory, and neuroprotection against Alzheimer's disease. Few of the derivatives exhibit rodenticidal, herbicidal, insecticidal properties [25-31], some of them shown urease-inhibitory properties [32] in addition to inhibit GlyT1 [33]. They also inhibit cholinesterase and

have anti-β amyloid aggregation properties. They have also shown teratogenic and embryotoxic effects [34].These chemicals also have anti-allergic [35], anti-hepatitis, and anticoagulant [36-37].

"Molecular docking" is a sort of structure-based drug design that can accurately anticipate how small molecule ligands will attach to a certain target binding site. The binding sites are assumed to be stiff macromolecules, in contrast to the ligand's flexibility [38-39]. Conformational generation was used to create every potential conformer for the ligand. Next, each conformer's optimal fitness was evaluated while it was affixed to the receptor's binding sites. The molecular docking mechanism is influenced by several variables that also impact drug-receptor interactions. Hydrogen bonding, hydrophobicity, dihedral angle, bond length, electrostatic forces, and steric hindrances are some of these variables [40].

The study of molecular attributes, such as structural changes [41], molecular structure stability [42], molecule involvement in chemical reactions [43], and dynamic events at the atomic level [44], is accomplished via the use of molecular dynamics (MD). The interactions and stability of the moving protein-ligand complex were determined by means of a molecular dynamics simulation.

Molecular dynamics simulations can calculate complicated interaction energies and provide light on the ligand binding process. The orthorhombic box containing a pre-measured volume of solvent solution was filled with the manually built receptor-ligand combination. After that, simulations were run for a short 100 nanosecond period with constant temperature and pressure. The interactions between the protein in its flexible and rigid forms were evaluated by comparing the outcomes of molecular docking experiments with MD simulations.

These compounds may help cure tuberculosis and address the issue of drug-resistant forms of the disease.

In this context, the aim of study is to find out the possible drug leads of our previously synthesized 1, 3-indanedione derivatives that are effective against tubercular bacilli by using computational tools. Based on the selection criteria, we performed molecular docking and molecular dynamics simulation (MDS) study on 15 derivatives that are reported to have anti-tubercular activity. These compounds have the ability to bind to the Mycobacterium tuberculosis InhA protein, which suggests that they might be employed as anti-tubercular medications to treat the H37Rv strain of the disease [45]. Molecular docking and dynamics simulations were used to examine the interactions between the M. tuberculosis InhA protein (receptor) and the 1,3-Indanedione molecule (ligand) at the active site.

Materials and Methods

Molecular docking

Ligand preparation

The Indane-1, 3-dione derivative compounds listed in Table 1 were initially designed using ChemDraw and saved in the Structural Data File (SDF) format. Subsequently, these compounds were converted into ligands using Autodock Vina 1.1.2 and PyRx Virtual Screening Tool 0.8 software, specifically the Chimera version 1.10.2 [46]. This preparation aimed to assess their binding affinity with the 2x23 enzyme. Further analysis of the compounds was conducted using Schrödinger's Maestro software [47]. The molecular structures of both the original ligand and the derivatives prepared as per proposed reaction scheme shown in Scheme 1. From this 2-(aryl methylene)-(1*H*)-indane-1,3-(2*H*)-diones were constructed using ChemDraw Ultra 8.0 version, with molecular structures saved in the mol file format. To optimize energy, the Universal

Force Field (UFF) feature of the PyRx program was employed [48]. The crystallographic configuration of M. tuberculosis InhA (PDB–2x23) was obtained from the RCSB Protein Data Bank (https://www.rcsb.org/).

Prior to connecting each atom, polar hydrogen and Kollman charges were applied. The pdbqt extension was used to save the final structure. Then, each structure was stored in the.pdb format using the OpenBabelGUI web server [49]. A cubic grid box of 40 x 40 x 40 Å3 and spaced 0.708 Å apart was created. The box's center is located at 24.012, 78.820, and 20.320. This box contains the ligand binding site of the integrin by design. Using the AutoDock default settings, ten docked conformations per molecule were produced, and these conformations were used in the docking calculations. In the research, a genetic algorithm was analysed using energy calculations. The research aims to evaluate the hydrogen bond length and energy that binds the ligand to the receptor utilizing docked ligand conformations. The receptor with the ligand-binding site was shown using Chimera 1.11. Molecular docking tests were used to investigate the binding affinities of the Indane-1, 3-dione derivative and the M. tuberculosis InhA protein. A single low energy ring conformation was generated for each ligand, and the optimized ligands were used in docking studies.

Protein preparation

For molecular docking investigations the crystal structure of M. TB InhA in complex with native ligand 2-(o-Tolyloxy)-5-hexylphenol (PT70) with PDB-2x23 and resolution 1.81 A^0 was used, as shown in Figure 1.

The protein's three-dimensional structure (PDB ID: 2x23) was extracted from website RCSB Protein Data Bank (www.rcsb.org).

A mycobacterial protein 2x23 protein composed of two chains, A and B, which combine to create a homodimer along a crystallographic 2-fold symmetry axis. Chain A was used to produce a macromolecule having a sequence of 269 units. TCU, also known as 5-Hexyl-2-(2-methylphenoxy) phenol, is the primary ligand for 2x23.

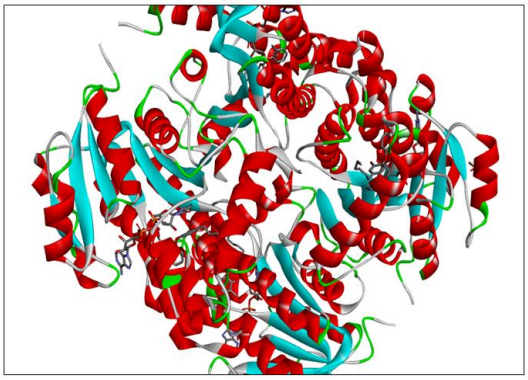

Figure 1. Crystal structure of M. tuberculosis InhA (PDB – 2x23) in complex with native ligand 2-(o-Tolyloxy)-5-hexylphenol (PT70) adapted from protein data bank.

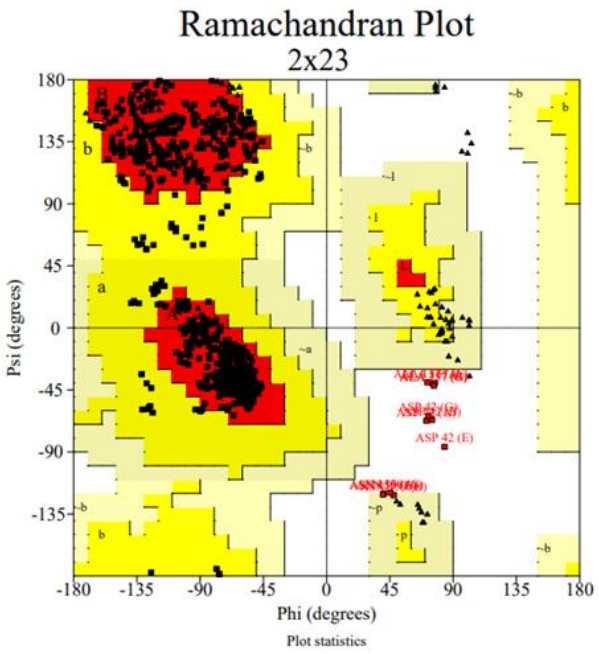

Figure 2. Ramachandran plot for M. tuberculosis InhA (2x23).

The Protein Preparation Wizard [50] in the Schrödinger software's Maestro [51] was used to construct and preprocess the protein complex. The complex was further reduced until the root

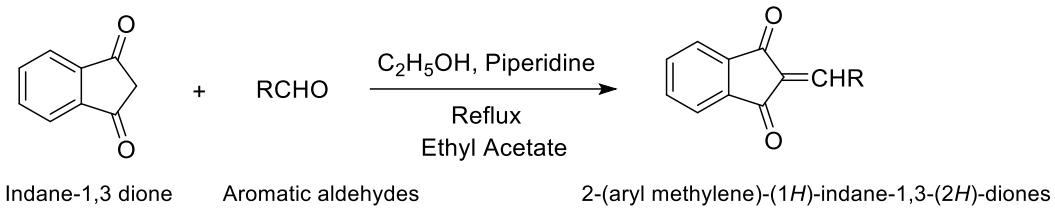

Scheme 1. Proposed reaction scheme for the synthesis of designed derivative.

mean square deviation (RMSD) reached 0.3 Å using the OPLS–2005 (Optimized Potential for Liquid Simulations) force field [52].

PROCHECK server predicts the Ramachandran Plot of protein model which was further validated by studying favourable and non-favourable regions [53]. The Ramachandran curve for the protein M. tuberculosis InhA (PDB ID: 2x23) was shown in Figure 2. This graphic shows that the highest concentration of amino acids is found in the optimum zone.

Protein–ligand interactions

A pdb file that was loaded into the LigPlot program was used to codify the protein-ligand interactions for a specific complex post-docking [54]. The two-dimensional interaction between the ligand and the protein's hydrophobic residues is shown in LIGPLOT. Intermolecular interactions, such as hydrogen bonds, hydrophobic contacts, and atom accessibilities, may be used to visualize the connection. Dotted lines are utilized to illustrate hydrophobic and hydrogen bond interaction schematics, respectively. The ligand atoms in touch with the proteins containing amino acid residues are shown as an arc with spokes extending toward them, and vice versa.

Molecular dynamic simulations

A study using molecular dynamic modelling (MD) was performed on the ligand-protein complexes exhibiting elevated docking positions. A 100 nanosecond duration of Molecular Dynamic (MD) stimulations was achieved using the Desmond module of the Schrödinger LLC software [55]. This study was conducted in order to confirm the changes occurring at the protein binding site and to evaluate these changes across the complex [56].

To simulate molecular dynamics, the starting state of receptor (protein) and ligand complexes was obtained by docking studies. The protein-ligand combination was pre-processed using Protein Preparation Wizard or Maestro, which incorporates sophisticated optimization and minimization. Every system was constructed using the software program System Builder. Among the indane-1, 3-dione derivatives, the greatest binding energy docked conformer was chosen for the MD simulations research using the OPLS 2005 force field. Using a preconfigured TIP3P water model, the protein–ligand pair was encased in an orthorhombic box [57]. The overall charge of the system was neutralized and the volume of the box was minimized by adding Na+ and Cl-ions. A Nose–Hoover thermostat [58] and a Martyna–Tobias–Klein barostat [59] were used to keep the temperature and pressure at 300 K and 1.01325 bar. The MD simulations were performed with consideration for the timescale, pressure, and atomic number using the NPT (Number of Atoms, Pressure, and Temperature) ensemble. During the simulations, the long-range electrostatic interactions were calculated using the Particle-Mesh-Ewald method [60]. An MD simulation was performed for 100 ns on the docked complex, writing coordinates at various intervals. Finally, in order to do a comprehensive examination, trajectories of simulated systems were generated. Using the Desmond module of

the Schrodinger program, the following metrics were measured at various points along the trajectory: the radius of gyration (Rg), the root-mean-square deviation (RMSD), and the root-mean-square fluctuation (RMSF). For proteins whose structures have been anticipated due to need of crystallized structures, MD reenactment ponders are most regularly performed to see how the proteins can carry on in physiological situations through examination of their stabilities in a recreation environment [61].

The variation in a protein atom's structure during molecular simulation is displayed by RMSD. A more stable system is indicated by a low RMSD in a simulation result. The RMSD graph exhibits oscillations throughout when a ligand interacts with the target protein structure, suggesting instability [62-63].

ADMET prediction

The designed compounds approachability can be described by ADME properties, described by Lipinski's rule of five [64].

The rule states that:

1) A molecular weight of fewer than 500 daltons,

2) No more than five donors of hydrogen bonds,

3) Ten hydrogen bond acceptors maximum,

4) An octanol-water partition coefficient log P not greater than 5 (lipophilicity, expressed as LogP), and

5) Molar refractivity should lie within range 40-130.

The Swiss Institute of Bioinformatics' (Switzerland) ADME webserver allowed users to paste the molecules' Simplifed Molecular Input Line Entry System (SMILES) to predict the drug-likeness parameters and pharmacokinetics (absorption, distribution, metabolism, excretion, and toxicity) of the 15 selected Indane-1, 3-dione derivatives [65-66], we utilized the online tool Molinspiration cheminformatics. This tool was employed to assess the drug similarity and bioactive ratings of the compounds. The online application admetSAR 2.0 was utilized to forecast the distribution, toxicity, and LD50 [67]. Drug molecules which show higher HIA absorb well when orally administered. For explaining mutagenicity of ligands AMES toxicity parameter used. TPSA or PSA reflecting penetrating ability of a drug in to cell membrane during a biochemical reaction. It should lie within limit of not greater than 140Å which have less penetrating power and high penetration when it lies below 60Å [68].

The STopTox website's toxicity prediction for chemicals 1, 4, 9, 11, and 15 also highlighted specific portions that was associated with increased or decreased acute inhalation toxicity and cutaneous sensitization (https://stoptox.mml.unc.edu/) [69].

Results and Discussion

Molecular docking studies

Autodock vina performed docking experiments of suggested Indane 1, 3 dione derivatives to protein active sites in order to determine the ligands' binding affinities to the protein. The generated compounds were docked into the M. tuberculosis InhA (2x23) strain to assess their antitubercular efficacy. Compounds 1 through 15 showed excellent affinity to the 2x23 receptor when compared to the anti-tubercular standard medication isoniazid. It was predicted that the different regions would serve as the analogues' and the target protein's primary docking sites. The docking data indicates that drugs and their analogues bind into the same binding region of the receptor. To learn more about the structural basis of the target protein's function, indane dione linked analogues were docked into its active domain. A connection was discovered through the computation of the total binding energy. The outcomes of the docking process are presented in Table 1.

Table 1. Docking score of Indane- 1, 3-dione derivatives

Compound Code	Docking score
01	**-10.054**
02	-7.3
03	-7.341
04	**-9.302**
05	-3.163
06	-7.314
07	-7.783
08	-8.412
09	**-9.287**
10	-8.296
11	**-10.38**
12	-8.747
13	-8.547
14	-6.497
15	**-8.413**
5-Hexyl-2-(2-methylphenoxy)phenol (TCU)	**-10.465**
Isoniazid	-5.894

A larger negative value of total binding energy indicates more affinity for the ligand-receptor binding. The docking investigations indicate that lipophilic substances and hydrogen bonds are largely in charge of the interactions. Our computational docking investigation revealed that 15 of the docked compounds, with binding efficiencies ranging from -3.16 to 10.38 kcal/mol, were more effective at binding than the positive control drug. This illustrated the chemicals' extraordinary power even further.

To determine the binding affinities and binding scores of the derivatives interactions with the amino acid residues present in the active pocket have been considered. Robust binding scores and remarkable binding affinities found while analysing results amongst majority of compounds. Out of total 15 compounds, compounds 1, 4, 9, 11, and 15 shown highest binding energies compared to the standard drug isoniazide which have binding energy of -5.894 kcal/mol. Accordingly, we selected this compounds for further investigation. Significantly, compound 11 has the highest binding energy (– 10.38 Kg/mol). The optimal configuration for compound 11 was then selected, followed by an in-depth analysis of binding and non-binding interactions counting a total of eleven hydrogen bond interactions with amino acids.

Scheme 2 displayed the 2D and 3D docking positions of the optimal conformer for compounds 1, 4, 9, 11, and 15.

The **compound 1** shown binding affinity **-10.054** and further analysis of ligplot-generated files revealed that 11 hydrogen bond interactions with amino acids with TYR158, ASP64, VAL65, ALA198, SER20, GLY96, THR196, ILE21, ILE194, GLY14, ILE95, LYS165(2), and 20 hydrophobic interaction with amino acid MET103, MET98, ILE202, PHE97, VAL203, MET199, LEU63, PHE41, MET161, LEU63, PHE149, ILE122, SER94, ILE15, ILE16, ASP148, GLY192, ALA191, MET147, LEU197, and PRO193 .**Compound 4** showed binding affinity **9.302** and 21 hydrophobic interactions with amino acids LEU63, SER94, MET161, PHE41, ILE215, GLN214, MET155, ILE122, SER94, PHE97, ILE15, ILE202, ILE16, ILE197, PRO193, MET147, ALA191, GLY192, ASP148, ALA157, and 11 hydrogen bond interactions with amino acids with ILE21, ILE194, LEU218, ASP64, GLY96,

SER20, ALA198, GLY14, ILE95, LYS165, and LEU218, respectively.

Compound 9 showed binding affinity **-9.287** and 22 hydrophobic interaction with amino acid LEU218, PRO156, ILE202, MET98, MET103, VAL203, MET199, MET161, PHE149, PHE41, GLY96, ALA198, SER94, ILE15, ILE16, LEU197, PRO193, ILE194, ALA191, MET147, ASP148, GLY192, and 11 hydrogen bond interactions with amino acids with amino acids like TYR158, ,LYS165, ILE95, GLY14, GLY96, ASP64, VAL65, ALA198, THR196, ILE21, and ILE194.

Compound 11 showed highest binding affinity i.e. **-10.38** and Compound 11 is forming 11 hydrogen bond interactions with amino acids ILE21, ILE194(2), GLY14, ASP 645, VAL165, GLY96, SER20, ALA198, THR196, LE95, and LYS(2).

There are total 22 non-bonded interactions formed by Compound 11 with amino acid ILE202, MET98, MET103, PHE97, VAL203, MET199, LEU218, TYR158, MET161, LEU63, PHE149, ILE122, SER94, ILE15, ILE16, ASP148, GLY192, ALA191, MET147, LEU197, and PRO193, respectively.

Compound 15 has binding affinity of **-8.413** and 23 hydrophobic interaction with amino acid MET155, MET199, VAL203, TYR158, LEU218, PHE97, ILE202, MET98, MET103, MET161, PHE41, LEU63, PHE149, ILE122, SER94, ILE15, ILE16, LEU197, PRO193, MET147, ALA191, GLY192, and ASP148. From docking study, total 11 hydrogen bonds formed by compound 15 with amino acid ASP64, VAL165, GLY96, SER20, ALA198, THR196, ILE21, ILE194, GLY14, ILE95, and LYS165 respectively. The corresponding bond lengths of respective hydrogen bonds were presented in a table.

The docking simulation disclosed that the title analogues exhibited favourable interactions with M. tuberculosis InhA (2x23), as illustrated in Scheme 2.

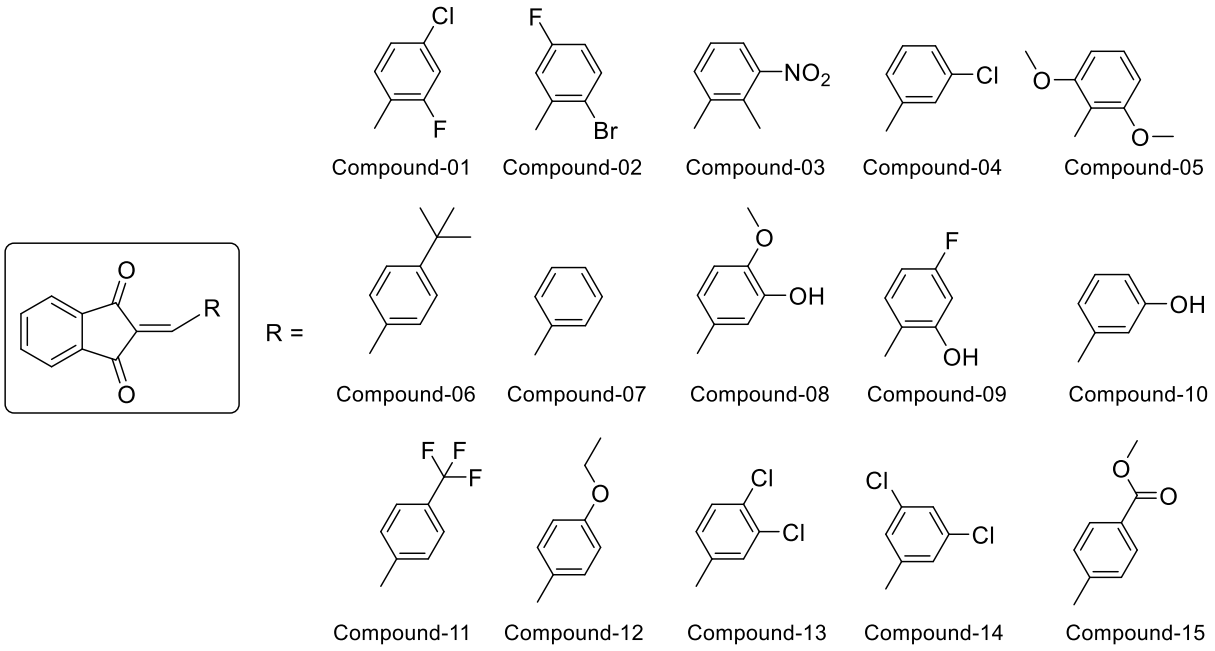

Scheme 2. Structures of designed compounds (1-15).

Table 2. Molecular interactions of ligands with amino acids of proteins

Ligand	Bond length (A0)	Active amino residues	Hydrophilic Interactions	Hydrophobic Contacts	No. of H-Bonds
1	3.06 3.14 3.12 3.18 2.52 3.27 2.77 2.89 2.58 3.05 2.72 3.21 2.90 2.70	TYR158 ASP64 VAL65 ALA198 SER20 GLY96 THR196 ILE21 ILE194 GLY14 ILE95 LYS165	ILE194, ILE21, LYS165, ILE95, ALA198, SER20, GLY96, ASP64, TYR158, and GLY64	MET103, MET98, ILE202, PHE97, VAL203, MET199, And LEU63. PHE41, MET161, PHE149, ILE122, ASP148, GLY192, ALA191, MET147, PRO193, ILE16, LEU197, ILE15, and SER94	12
4	2.89 3.05 2.58 2.57 3.14 3.27 2.52 3.18 2.72 3.21 2.90 2.70 2.57	ILE21 ILE194 LEU210 ASP64 GLY96 SER20 ALA198 GLY14 ILE95 LYS165 LEU218	ILE21, ILE194, LEU218, ASP64, GLY96, SER20, ALA198, GLY14, ILE95, LYS165, and LEU218	LEU63, SER94, MET161, PHE41, ILE215, GLN214, MET155, ILE122, SER94, PHE97, ILE15, ILE202, ILE16, ILE197, PRO193, MET147, ALA191, GLY192, ASP148, and ALA157	11
9	2.93 2.90 2.70 3.21 2.72 3.23 3.14 3.12 3.18 2.77 2.89 3.05 2.58	TYR158 LYS165 ILE95 GLY96 GLY96 ASP64 VAL65 ALA198 THR196 ILE21 ILE194	TYR158, LYS165, ILE95, GLY14, GLY96, ASP64, VAL65, ALA198, THR196, ILE21, and ILE194	LEU218, PRO156, ILE202, MET98, MET103, VAL203, MET199, MET161, PHE149, PHE41, GLY96, ALA198, SER94, ILE15, ILE16, LEU197, PRO193, ILE194, ALA191, MET147, ASP148, and GLY192	11

Table 2. Continued…

Ligand	Bond length (A0)	Active amino residues	Hydrophilic Interactions	Hydrophobic Contacts	No. of H-Bonds
11	3.14 3.12 3.27 2.52 3.18 2.77 2.89 2.90 2.70 2.72 3.21 3.05 2.58	ASP645 VAL165 GLY96 SER20 ALA198 THR196 ILE21 LYS165 GLY14 ILE95 ILE194	ASP645, VAL165, GLY96, SER20, ALA198, THR196, ILE21, ILE194(2), GLY14, ILE95, and LYS(2)	ILE202, MET98, MET103, PHE97, VAL203, MET199, LEU218, TYR158, MET161, LEU63, PHE149, ILE122, SER94, ILE15, ILE16, ASP148, GLY192, ALA191, MET147, LEU197, and PRO193	11
15	3.27 3.18 3.14 3.12 2.58 3.05 2.52 3.21 2.77 2.89 2.70 2.90 2.72	GLY96 ALA198 ASP645 VAL165 ILE194 SER20 ILE95 THR196 ILE21 LYS165 GLY14	ASP64, VAL165, GLY96, SER20, ALA198, THR196, ILE21, ILE194, GLY14, ILE95, and LYS165	MET155, MET199, VAL203, TYR158, LEU218, PHE97, ILE202, MET98, MET103, MET161, PHE41, LEU63, PHE149, ILE122, SER94, ILE15, ILE16, LEU197, PRO193, MET147, ALA191, GLY192, and ASP148	11

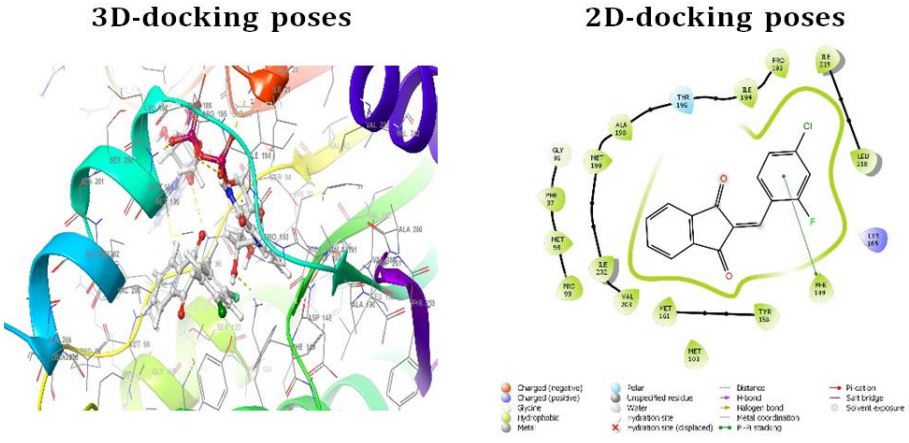

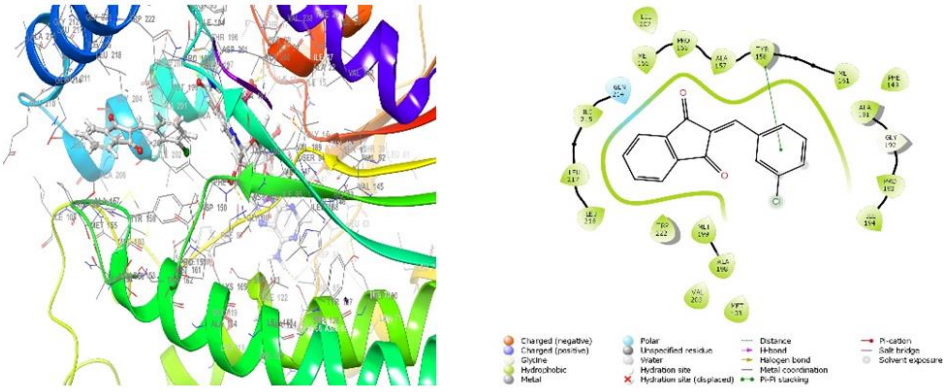

Compound 4

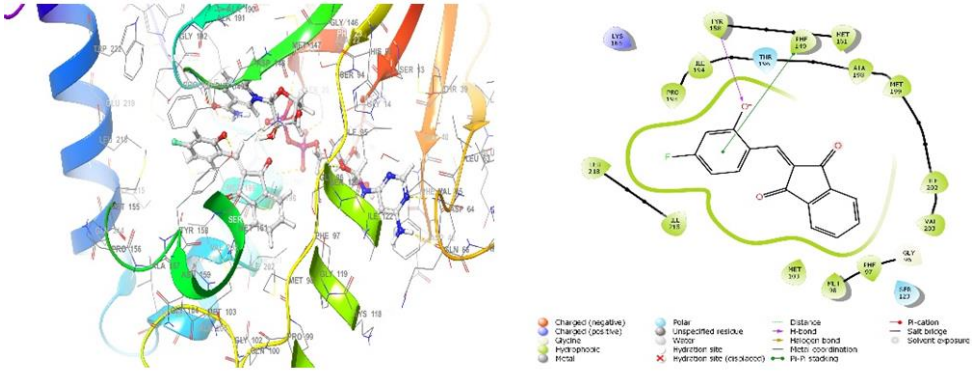

Compound 9

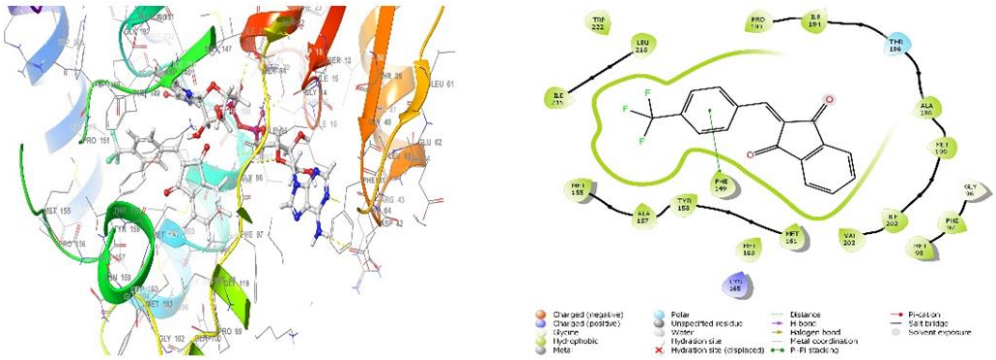

Compound 11

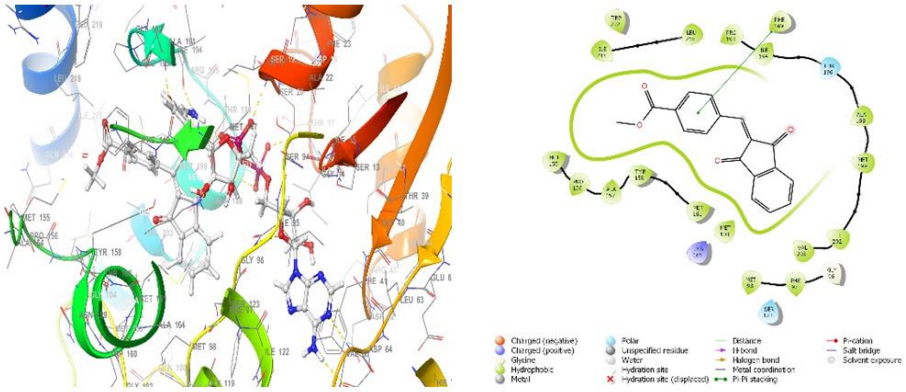

Compound 15

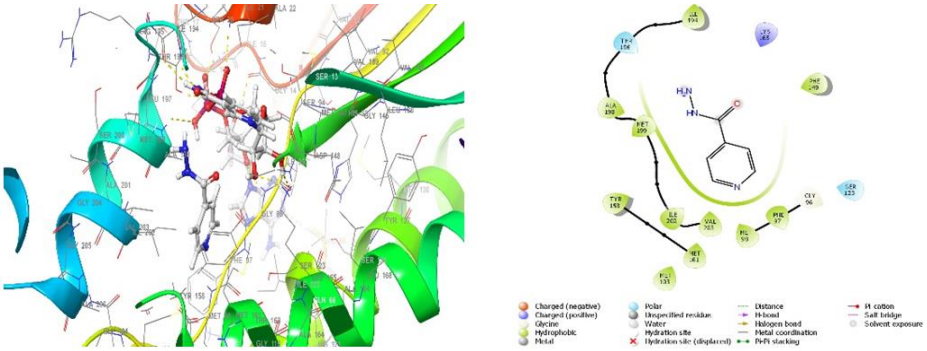

ISONIAZID

Figure 3. Three-dimensional and two-dimensional docking poses of the five most active compounds

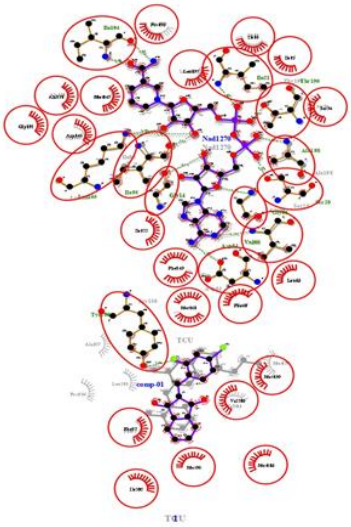

Compound 1

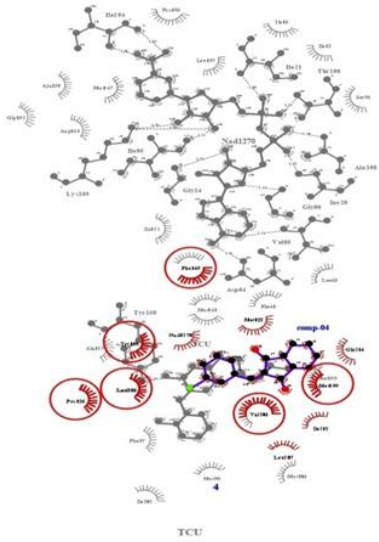

Compound 4

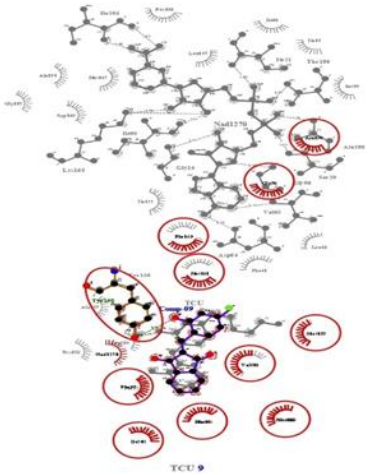

Compound 9

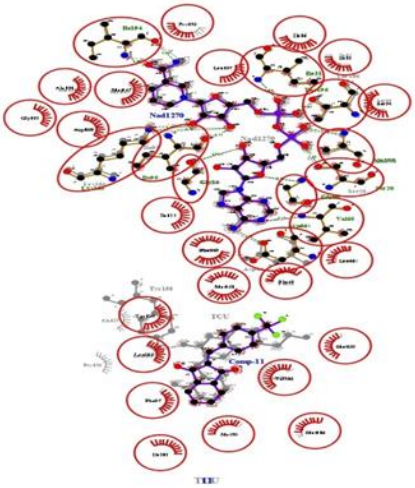

Compound 11

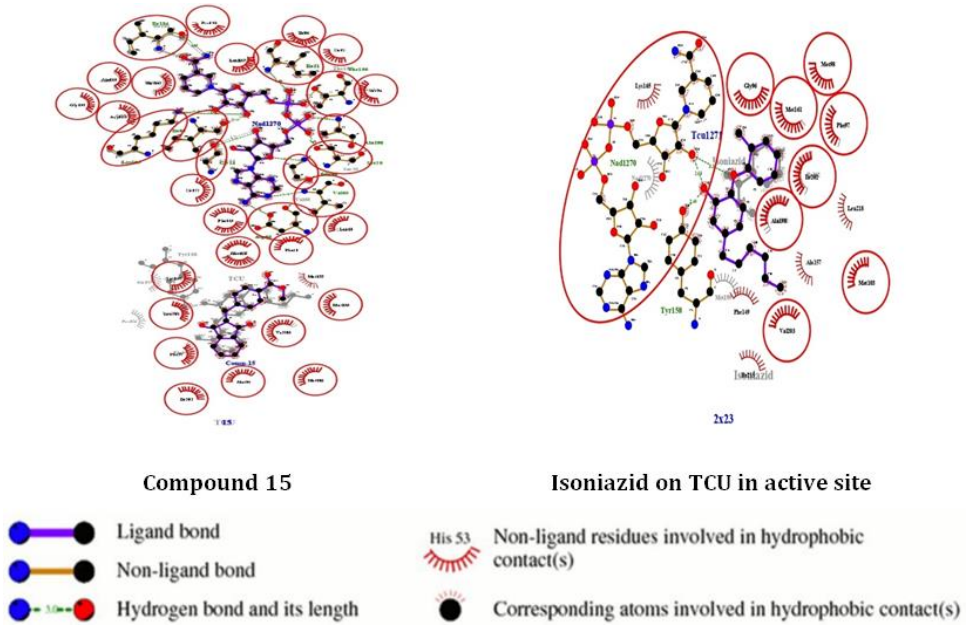

Figure 4. LigPlot+ to show molecular interaction between lead compounds (with the amino acid residue of M. tuberculosis InhA protein (2x23). Green coloured dashed lines indicate H-bonds between ligand and residue of amino acid. The spoked arcs indicate residues non-bonded contacts formed with the ligand molecule.

ADMET studies

The drug similarity and bioactive scores were determined using Molinspiration cheminformatics and the SwissADME webserver, while the *in silico* pharmacokinetic characteristics of the compounds were predicted using the AdmetSAR online tool. The ACD/ChemSketch software was utilized to create 2D structural models of the developed molecules. SMILES notations were assigned to both the molecules and standard medicines, which were then utilized to estimate individual ADMET, bioactive, and drug similarity scores. AdmetSAR offers insights into both active compounds and the elimination of large molecules with undesirable functional groups that may be physiologically flawed. The biological relevance of a molecule's region is determined by its shape, surface area, and fingerprint qualities, all of which are considered in the comprehensive analysis of significant molecules. Additional characteristics contributing to understanding the metabolic drug mechanism of the proposed compounds include blood-brain barrier penetration, intestinal absorption, hepatotoxicity, water solubility, and CACO-2 cell permeability. It is noteworthy that the compounds adhere to the Lipinski Rule of Five. In contrast to large molecular weight substances, low molecular weight molecules are more readily absorbed, dispersed, and transported. The bulkiness of molecules increases proportionately with molecular weight, up to a certain limit.

Topological Polar Surface Area, or TPSA, is a highly helpful physicochemical metric for molecules that provides information about the polarity and transport capabilities of various compounds. The total amount of polar atoms, mostly nitrogen and oxygen as well as hydrogen atoms connected to a ring structure, makes up the polar surface area. Table 7 presents the bioactivity ratings of the compounds, which were designed as G-protein coupled receptor (GPCR) ligands, ion channel modulators, nuclear receptor ligands, kinase inhibitors, protease inhibitors, and enzyme inhibitors. A compound is considered inactive if its bioactivity score is less

than -0.50, while scores ranging from -0.50 to 0.00 suggest moderate activity. Compounds with scores greater than 0.00 are likely to exhibit significant biological activity. In comparison to other strategies, enzyme inhibition bioactivity scores tend to approach 0.0.

Table 3. *In-silico* ADMET screening for the proposed compounds (1-15)

Compound No.	Molecular weight g/mol	Num. rotatable bond	Num. H-bond acceptors	Num. H-bond donors	Molar Refractivity	TPSA Å²	Consensus Log Po/w	Log Kp (skin permeation) cm/s	Lipinski Rule	Violation	Pharmacokinetics	
											GI absorption	BBB permeant
Comp-1	286.68	1	3	0	74.49	34.14	3.85	-5.05	Yes	0	High	Yes
Comp-2	331.14	1	3	0	77.18	34.14	3.93	-5.27	Yes	0	High	Yes
Comp-3	279.25	2	4	0	78.34	79.96	2.40	-5.64	Yes	0	High	No
Comp-4	268.69	1	2	0	74.53	34.14	3.55	-5.01	Yes	0	High	Yes
Comp-5	294.30	3	4	0	82.51	52.60	2.98	-5.65	Yes	0	High	Yes
Comp-6	290.36	2	2	0	88.79	34.14	4.21	-4.40	Yes	0	High	Yes
Comp-7	234.25	1	2	0	69.52	34.14	3.00	-5.24	Yes	0	High	Yes
Comp-8	282.27	2	4	0	75.97	43.37	3.32	-5.49	Yes	0	High	Yes
Comp-9	280.27	2	4	1	78.04	63.60	2.61	-5.79	Yes	0	High	Yes
Comp-10	250.25	1	3	1	71.55	54.37	2.58	-5.59	Yes	0	High	Yes
Comp-11	302.25	2	5	0	74.52	34.14	4.05	-5.03	Yes	0	High	Yes
Comp-12	278.30	3	3	0	80.82	43.37	3.31	-5.27	Yes	0	High	Yes
Comp-13	303.14	1	2	0	79.54	34.14	4.06	-4.77	Yes	0	High	Yes
Comp-14	303.14	1	2	0	79.54	34.14	4.08	-4.77	Yes	0	High	Yes
Comp-15	292.29	3	4	0	80.80	60.44	2.95	-5.70	Yes	0	High	Yes

Table 4. Predicted biological permeability of standards and synthesized Indane 1.3 dione derivatives using admet SAR

Compound No.	Blood Brain Barrier	Human Intestinal Absorption	CACO2 Permeability	Renal Organic Cation Transporter	AMES Toxicity	Biodegradation
	Probability	Probability	Probability	Probability	Probability	Probability
Comp-1	0.7000	1.0000	0.8369	1.0000	0.6200	0.9250
Comp-2	0.6750	1.0000	0.8412	1.0000	0.5200	0.8750
Comp-3	0.5250	0.9901	0.7754	1.0000	0.7200	0.9500
Comp-4	0.6750	1.0000	0.9098	1.0000	0.6500	0.8250
Comp-5	0.5750	1.0000	0.8672	1.0000	0.6700	0.9000
Comp-6	0.7000	1.0000	0.7901	0.9250	0.6200	0.8500
Comp-7	0.5750	1.0000	0.7805	1.0000	0.5000	0.7250
Comp-8	0.5750	0.9972	0.7763	1.0000	0.5700	0.9250
Comp-9	0.5750	1.0000	0.9361	1.0000	0.6100	0.9500
Comp-10	0.7000	1.0000	0.6972	1.0000	0.5100	0.8750
Comp-11	0.7000	1.0000	0.5966	1.0000	0.5200	0.9000
Comp-12	0.5500	1.0000	0.7366	0.8000	0.5500	0.8250
Comp-13	0.6750	1.0000	0.8551	1.0000	0.7300	0.9250
Comp-14	0.6750	1.0000	0.7840	1.0000	0.6000	0.9000
Comp-15	0.5750	1.0000	0.6705	0.9750	0.6000	0.7750

Table 5. Predicted biological permeability of standards and synthesized Indane 1.3 dione derivatives using admet SAR

Compound No.	P-Glycoprotein Substrate Probability	CYP-3A4 Inhibitors Probability	CYP-2D6 Inhibitors Probability	CYP Inhibitory Promiscuity Probability	HERG Inhibition Probability
Comp-1	0.8056	0.5101	0.7758	0.7999	0.5158
Comp-2	0.9580	0.5850	0.7635	0.8031	0.6278
Comp-3	0.9525	0.5220	0.8113	0.7420	0.7501
Comp-4	0.8289	0.5276	0.7732	0.8466	0.6029
Comp-5	0.9211	0.5468	0.7104	0.9319	0.5173
Comp-6	0.9399	0.7676	0.8039	0.8598	0.4085
Comp-7	0.9844	0.7988	0.6444	0.8563	0.7091
Comp-8	0.9347	0.6862	0.8462	0.7493	0.7226
Comp-9	0.8704	0.7077	0.8764	0.8868	0.4272
Comp-10	0.9522	0.8626	0.8402	0.7458	0.8273
Comp-11	0.9608	0.7733	0.7687	0.6897	0.5320
Comp-12	0.9616	0.8827	0.8026	0.9683	0.6714
Comp-13	0.9851	0.5194	0.5972	0.8466	0.5335
Comp-14	0.9889	0.5194	0.5972	0.8466	0.5887
Comp-15	0.9153	0.7022	0.8640	0.8256	0.6963

Table 6. Predicted biological permeability of standards and synthesized Indane 1.3 dione derivatives using admet SAR

Compound No.	Carcinogens	Acute Oral Toxicity	Carcinogenicity (Three Class)	Rat Acute Toxicity LD50, Mol/Kg	Tetrahymena pyriformis Toxicity pIGC50 (Ug/L)
	Probability	Probability	Probability	Probability	Probability
Comp-1	0.7159	0.6425	0.4958	2.56	1.624
Comp-2	0.7780	0.4950	0.4072	2.311	1.363
Comp-3	0.5026	0.6436	0.4262	2.477	1.126
Comp-4	0.7159	0.6584	0.5073	1.961	1.72
Comp-5	0.8387	0.4176	0.5371	1.911	1.216
Comp-6	0.8566	0.5319	0.4715	2.241	1.364
Comp-7	0.8366	0.6333	0.5024	1.974	1.348
Comp-8	0.9074	0.3723	0.4333	1.288	1.255
Comp-9	0.7542	0.4233	0.4222	1.824	1.235
Comp-10	0.8166	0.5246	0.4281	1.829	1.195
Comp-11	0.8236	0.6056	0.4977	2.173	1.306
Comp-12	0.8766	0.5432	0.5102	1.798	1.077
Comp-13	0.7159	0.6584	0.5073	2.208	1.475
Comp-14	0.7159	0.6584	0.5073	1.69	1.781
Comp-15	0.8087	0.5022	0.4565	1.728	0.831

Table 7. Bioactivity scores of the series by using the Molinspiration Software

Compound	GPCR ligand	Ion channel modulator	Kinase inhibitor	Nuclear receptor ligand	Protease inhibitor	Enzyme inhibitor
Comp-1	-0.53	-0.78	-0.13	-0.35	-0.73	-0.29
Comp-2	-0.65	-0.81	-0.09	-0.52	-0.82	-0.28
Comp-3	-0.62	-0.74	-0.19	-0.42	-0.71	-0.32
Comp-4	-0.55	-0.72	-0.15	-0.45	-0.73	-0.23
Comp-5	-0.41	-0.66	-0.05	-0.28	-0.54	-0.22
Comp-6	-0.34	-0.56	0.00	-0.12	-0.46	-0.14
Comp-7	-0.63	-0.77	-0.17	-0.49	-0.76	-0.22
Comp-8	-0.45	-0.72	-0.03	-0.25	-0.62	-0.16
Comp-9	-0.51	-0.72	-0.06	-0.28	-0.70	-0.21
Comp-10	-0.50	-0.69	-0.07	-0.22	-0.67	-0.13
Comp-11	-0.31	-0.53	0.07	-0.08	-0.42	-0.15
Comp-12	-0.52	-0.77	-0.14	-0.28	-0.62	-0.26
Comp-13	-0.46	-0.68	-0.09	-0.37	-0.64	-0.21
Comp-14	-0.46	-0.67	-0.08	-0.38	-0.64	-0.21
Comp-15	-0.52	-0.76	-0.14	-0.29	-0.58	-0.25

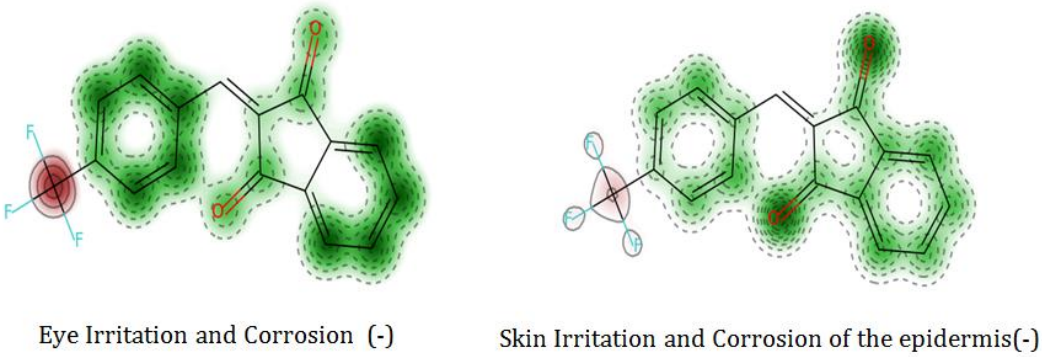

Figure 5. Acute inhalation toxicity of compound 11 (left) and skin sensitization (right).

In the analysis, toxic substances were denoted by a positive sign (+), while non-toxic compounds were marked with a negative sign (-) based on projected toxicities. Functional groups contributing to non-toxic features were highlighted in green, while those contributing to toxic traits were indicated in brown. As depicted in Figure 5, compound 11 was found to be non-toxic for skin irritation and epidermal corrosion, as well as eye irritation and corrosion.

Molecular dynamics simulation

The Desmond v5.6 program, integrated into the Schrödinger module 61, was employed to conduct molecular dynamics (MD) simulations. These simulations were conducted to monitor the stability of the protein-ligand complex structure and compare morphological changes occurring during protein-ligand interaction in its apo form. Root Mean Square Deviation (RMSD) was computed to assess stability, as depicted in Figure 6. Drug-enzyme complexes which shows the minimum binding energy, is ideal target for molecular dynamics (MD) simulation study. To explore the structural stability of compound 11-TCU complex, MD simulations were conducted at nanosecond time scales. MD simulations were performed for compound 11, the top-scoring molecule from docking experiments, and the co-crystallized inhibitor (TCU).

Understanding the receptor-ligand complex and the binding mechanism of compound 11 involved 100 ns MD simulations. The RMSD graph in Figure 6(a) demonstrates the graph displays protein RMSD on the left Y-axis and ligand RMSD on the right Y-axis.

Protein RMSD values ranged from 0.5 to 1.2 Å, while ligand RMSD values ranged from 1 to 2.4 Å, fluctuating between 20 ns and approximately 70 ns. The RMSD graph indicates that lower RMSD values correspond to higher stability of the protein-ligand complex.

For the 2x23-ligand complex, RMSD values remained steady for 10 ns, fluctuated for the next 10 ns, and then stabilized for 20 ns. The curve for compound 11 fluctuated for 60 ns before stabilizing around 1.25 Å.

Figure 6(a) displays the RMSD in Cα-atoms of 2x23 alone (teal color) or 2x23-ligand complex (brown line). Compound 11 induced the protein's RMSD to remain constant at 1.25 Å for the entire 70-ns simulation period, after which it rose to 1.50 Å and stabilized at 2.4 Å for the remaining 70 ns.

The RMSF graph (Figure 6(b)) illustrates the mobility of the target proteins; several peaks signify the presence of flexible amino acids on the protein's C-α backbone. Heat maps and histograms representing probable protein-ligand interactions are produced by MD simulations (Figure 6(c) and (d)). The interface between a ligand and protein is composed of four different forms of bonding: hydrogen bonds (green), ionic bonds (pink), water bridges (blue), and hydrophobic interaction (grey).

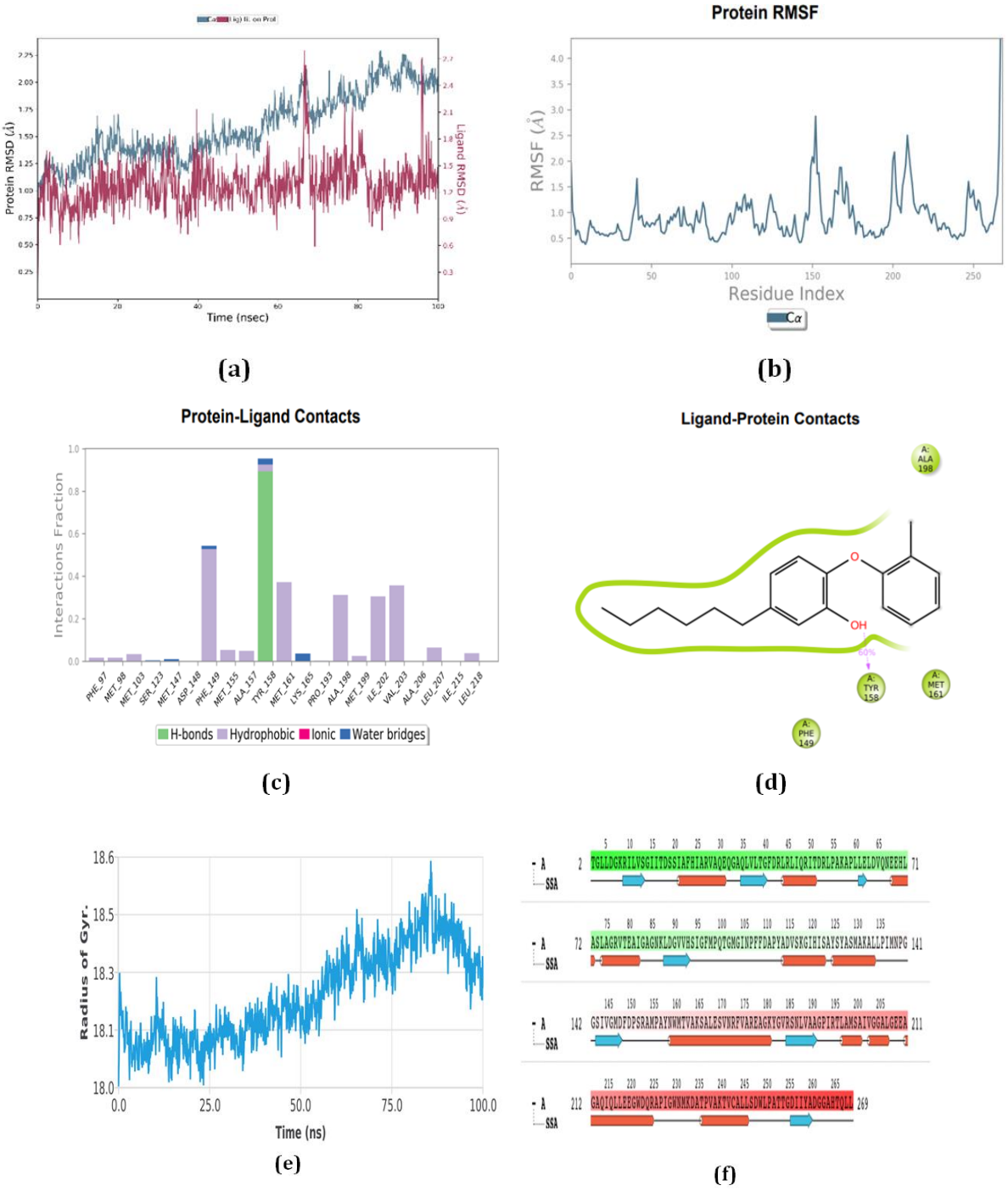

Figure 6. Protein 2x23-TCU Complex (a) Graphical representation of Protein RMSD (Å) 2x23alone (teal color) and Ligand RMSD (Å) versus time (ns), and in the presence of TCU (brown color) (b) Protein fluctuation study during simulation through RMSF, (c) Histogram representation specifies probable protein-ligand interactions, (d) Ligand protein contact. e) Radius of gyration Rg) of Cα backbone of 2x23 bound with TCU (f) Graphical illustration for protein A chain. 268 residues in Protein chain A of selected target protein, 4012 atoms, 1996 heavy atoms, and charge: -4, different colour shows pattern of SSA in 269 amino acid residues.

The amino acid residues (Figure 6(c)) show that Tyr158, Phe97, Met98, Met103, Phe149, Met155, Ala157, Met161, Ala198, Met199, Ile202, Val203, Leu207, Leu218, and Tyr158 create hydrophobic interactions (grey), whereas Met 147, Phe149, Tyr 158, and Lys165 form water bridges (blue), respectively. Moreover, the binding site residues vs. interaction fractions plot (c) (interaction fraction near to 1) shows that Tyr158 of the protein made several contacts. Sixty percent of the MD run was spent with TCU maintaining its solitary polar H bonding with Tyr158 (See Figure 6(d)).

More than 60.0% of the simulation time takes place during encounters within the specified trajectory range of 0.00 to 100.00 nanoseconds. A ligand's fundamental moment of inertia, or radius of gyration (rGyr), serves as a proxy for its "compactness." In this experiment, the 2x23 C-backbone's radius of gyration (Rg) in relation to the TCU-ligand dropped from 18.3 to 18.1 during the first 50 ns, rose to 18.5 over the next 80 ns, and then dropped to 18.3 again. When the gyration (Rg) decreases, the protein is heavily oriented inside a ligand-bound state (See Figure 6(e)).

The protein secondary structure elements (SSE) incorporates α-helices and β-strands distribution by residue index to whole protein structure and describes the SSE composition for each trajectory frame throughout the simulation time as shown in graph 8a and 8b. Careful moniteration was done over each residue and its SSE assignment for certain period of time through generated plots (Figure 7(a)). The total percentage of SSE - 2x23 in complex with TCU was observed 55% (α-helix = 32% and β-sheets = 23%), which was in harmony with the reported values of SSEs 52% (27% α-helix and 25% β-sheets) (upper panel, Figure 7 (b)).

The interaction of ligand TCU to active sites of 2x23 not altering priteins secondary structure, besides the involvement of each amino acid residue in the SSE formation of 2x23 as a function of simulation is also shown (Figure 7(b), lower panel). MD simulation results depicted in Figure 7(d), shown intermolecular interactions of the 2x23-protein-TCU complex and trajectory analysis reveals a minimum of two and a maximum of six contacts validates the molecular docking results.

During simulation study the total number of interactions in terms of contacts seen between 2x23-protein-TCU complex fluctuates in the 2–8 range, with 5 median contacts (Figure 7(d), upper panel). The amino acids residues Tyr158, Phe149, Ala198, and Ile202 were involved in most the simulation time making contact with TCU indicated in Figure 7(d), lower panel).

Here, various surface areas including solvent accessible surface area (SASA), molecular surface area (MolSA), and polar surface area (PSA) of ligand TCU in complex with M. tuberculosis InhA protein (2x23) were measured during the simulation to display the protein contacts to solvent molecules and approaches its conformational stability. A high values of SASA ranging 60–80 °A2, PSA 50–55 °A2, and MolSA of 315–320°A2 were also observed in the crystalized ligand, which helped to confirms stability throughout a 100 ns MD simulation time (Figure 7(f)). The identical protein forces to become more tightly pack and less flexible when the ligands were attaching to receptor.

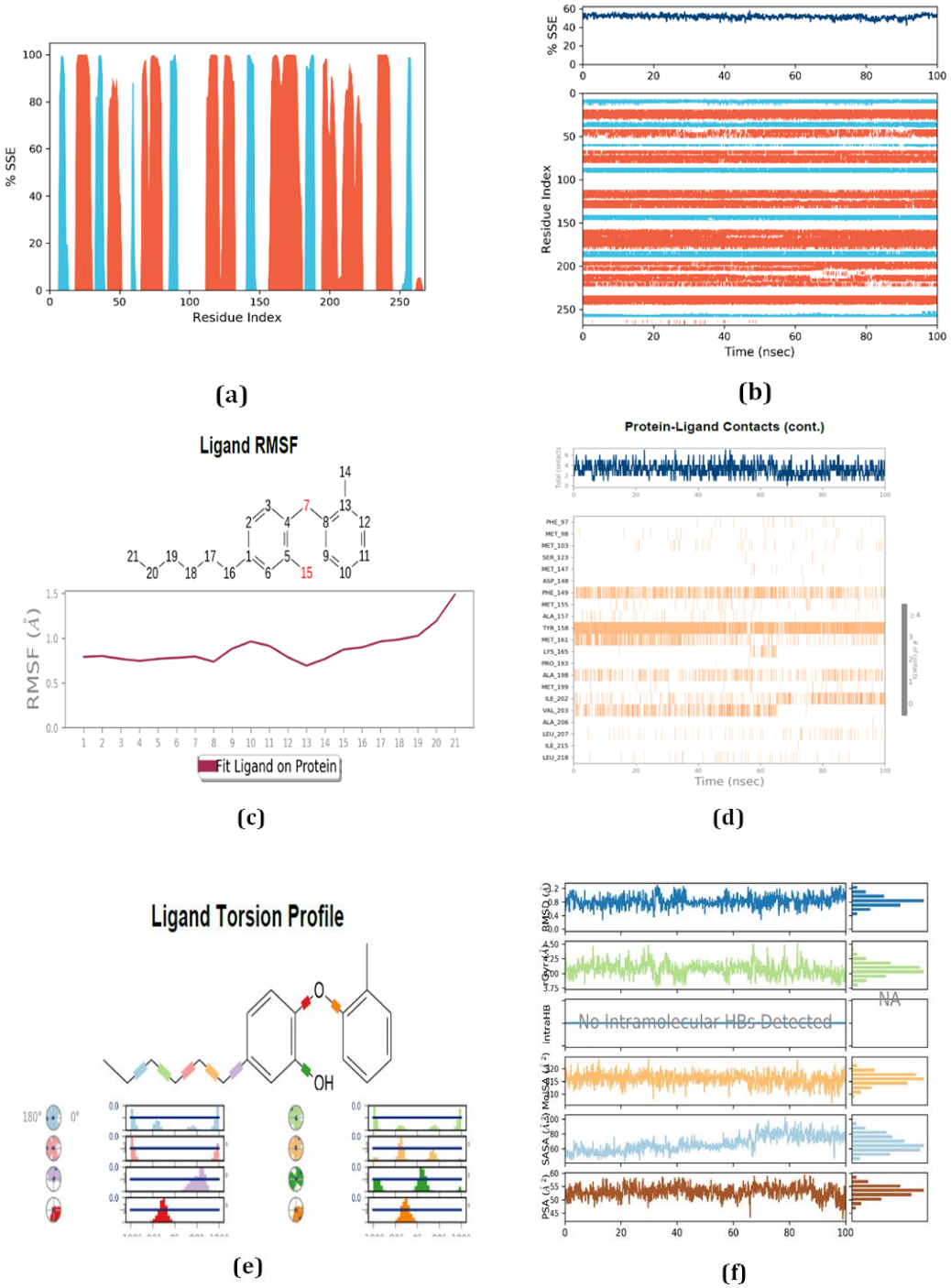

Figure 7. (a) Comparison of Secondary Structure Elements (SSE) between the TCU and crystallized ligand in Molecular Dynamics (MD) simulation. The Y-axis represents the TCU residue index and SSE, highlighting differences during the 60–65 nanoseconds MD simulation period. (b) TCU exhibits slight variation between 40–55 nanoseconds. (c) Representation of Ligand Root-Mean-Square Fluctuation (RMSF) and its interaction with 2x23. (d) Timeline depicting the total contacts between TCU and the 2x23-protein complex. (e) Torsion profile of the ligand TCU. (f) Ligand properties, including RMSD (Root-Mean-Square Deviation), MolSA (Molecular Surface Area), SASA (Solvent Accessible Surface Area), PSA (Polar Surface Area), rGyr (Radius of Gyration), and intraHB (Intramolecular Hydrogen Bonds). These properties indicate stability and characteristics of the ligand.

Whereas the RMSD values of ligands range from 1.2 to 3.5 Å, those of proteins range from 0.5 to 1.2 Å. There are other periods at which fluctuations happen, including 10 ns and around 20 ns (Figure 8(a)). Up to 10 ns, the complex RMSD values of 2x23-11 are stable. After that, oscillations take place. They do, however, stabilize once more between 10 and 20 ns. The stability of this chemical is demonstrated during a 20 nanosecond period. Variations continue until 0.5 Å is reached, at which point they increase to 1.5 Å.Up to 55 nanoseconds, the curve behaves consistently; beyond that, it drops to 0.6 angstroms. Finally, it was relatively stable up to a distance of 1.5 Å. The root mean square deviation (RMSD) of the Cα atoms in the 2x23 molecule, either alone (teal color) or in conjunction with 2x23-11 (brown line), is shown in Figure 8(a). For the entire 20-ns simulation period, the protein's root mean square deviation (RMSD) in the presence of 11 stayed constant at about 1.25Å. It then went up from 1.25 to 2.1 Å, and then it remained at 3.5 Å for 25 ns. Root mean square fluctuations (RMSF) are used to analyse residue flexibility in the context of ligand binding studies. The range of values for the root mean square fluctuation (RMSF) is 1.5 to 4.2 angstroms (Å). The mobility of target proteins is depicted in the RMSF graph Figure 8(b), where many peaks signify the existence of flexible amino acids on the protein's C-α backbone.

Proteins have RMSD values between 0.5 and 1.2 Å, while ligands have values between 1.2 and 3.5 Å. Variations are seen in these data at different time intervals, such as around 20 ns and 10 ns (Figure 8(a)). The complex RMSD values of 2x23-11 are steady for up to 10 ns; oscillations then begin and persist for up to 20 ns. This chemical's stability is shown throughout the course of 20 nanoseconds. The variations increase to 1.5 Å after first reaching a value of 0.5 Å. The graph behaves consistently for 55 nanoseconds, after which it again drops to 0.6 angstroms. Ultimately, it remained comparatively constant for 1.5 Å.

Figure 8(a) displays the root mean square deviation (RMSD) of the Cα atoms of the 2x23 protein either in isolation (teal color) or in conjunction with 2x23-11 (brown line). The protein's root mean square deviation (RMSD) in the presence of 11 remained constant at around 1.25Å for the duration of the 20-ns simulation session, and then it increased from 1.25 to 2.1 Å before staying at 3.5 Å for 25 ns. In the context of ligand binding investigations, residue flexibility is analysed using root mean square fluctuations (RMSF). The RMSF value falls between 1.5 and 4.2 angstroms (Å). The RMSF graph Figure 8(b), which shows many peaks indicating the presence of flexible amino acids on the protein's C-α backbone, illustrates the mobility of target proteins.

Figure 8(c) shows the interactions and contacts (hydrophobic, ionic, water bridges, and H-bonds) in chronological order. The upper panel displays the total number of distinct interactions that have happened throughout the trip between the ligand and the protein. The lower panel especially looks at the residues that interact with the ligand in each frame of the trip. Certain residues produce a wide variety of interactions with the ligand, which are represented by a greater shade of orange on the color scale on the right side of the graph.

Hydrophobic interactions are exhibited by Leu218, Met198, Met103, Phe149, Met161, Ala157, Met161, Ile202, Val203, Leu218, and Pro193. On the other hand, a hydrogen bond is implicated between amino acid residues Lys165 and Tyr158 (green). Blue water bridges are also formed by Tyr158, Ala198, Lys165, and Gln100. Figure 8(c). Furthermore, as the graph (c) illustrating the relationship between interaction percentages and binding site residues (with an interaction fraction of 0.6) demonstrates, Phe149 of the protein created several links. Compound 11 was able to hold onto its two polar hydrogen bonding connections with tyrosine 158 and lysine 165 for sixty percent of the molecular

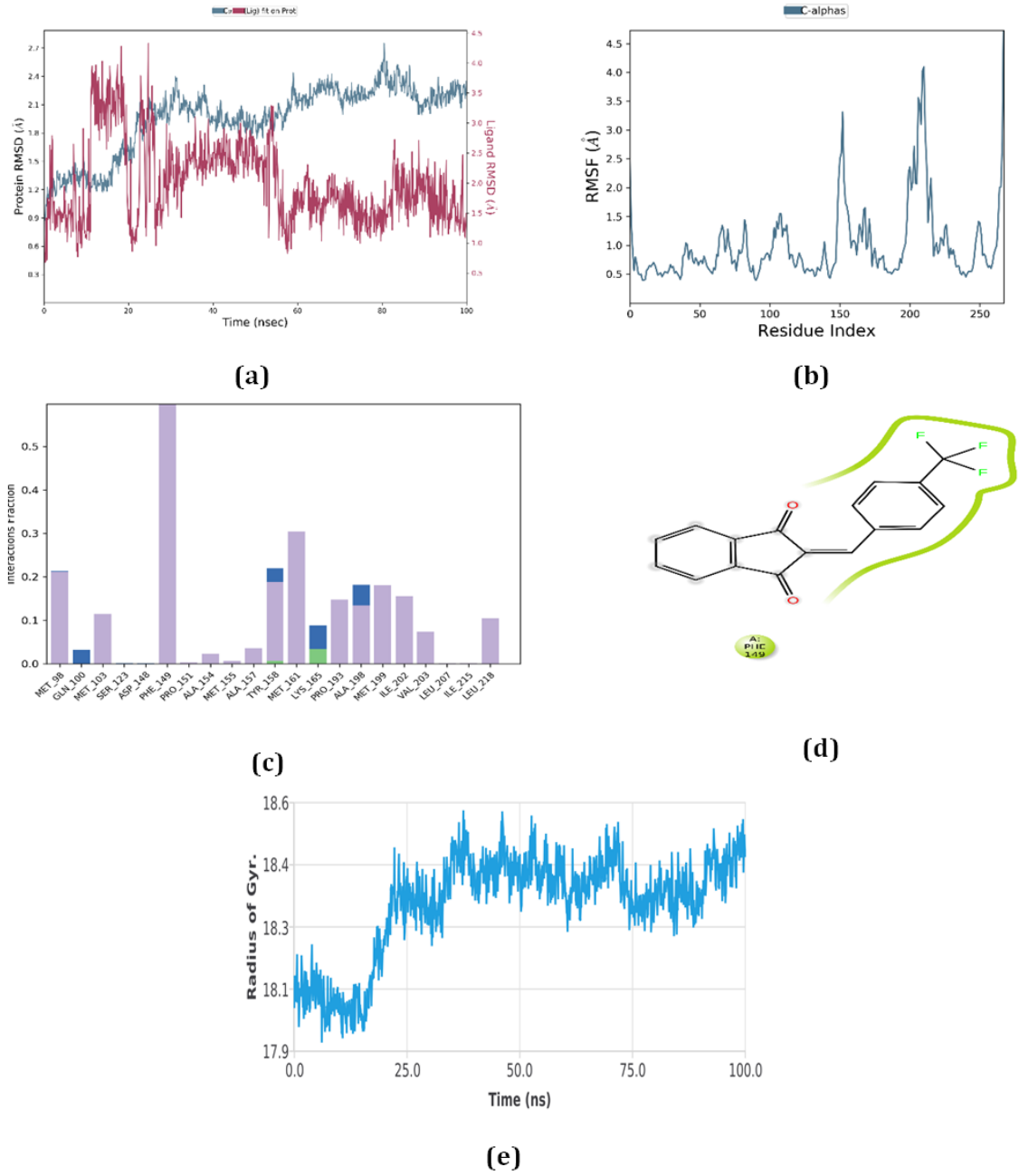

Figure 8. Protein **2x23-Compound 11** Complex (a) Graphical representation of Protein RMSD (Å) 2x23alone (teal color) and Ligand RMSD (Å) versus time (ns), and in the presence of **11** (brown color) (b) Graphical representation of RMSF (Å) versus the residual index, (c) Histogram representation specifies probable protein-ligand interactions, (d) Ligand protein contact. e)Radius of gyration Rg) of Cα backbone of 2x23 bound with Protein **2x23-Compound 11.**

dynamics simulation. For additional information, refer to Figure 8(d). Figure 8(d) illustrates interactions occurring for more than 30.0% of the simulation time within the specified trajectory range of 0-100.00 nanoseconds. The radius of gyration (Rg) of the 2x23 C-backbone attached to the 11 decreased from 18.1 to 18 in the first 12 nanoseconds of this experiment. Then, in the next 13 ns, it increased to 18.4, and by the time it reached 30 ns, it had decreased to

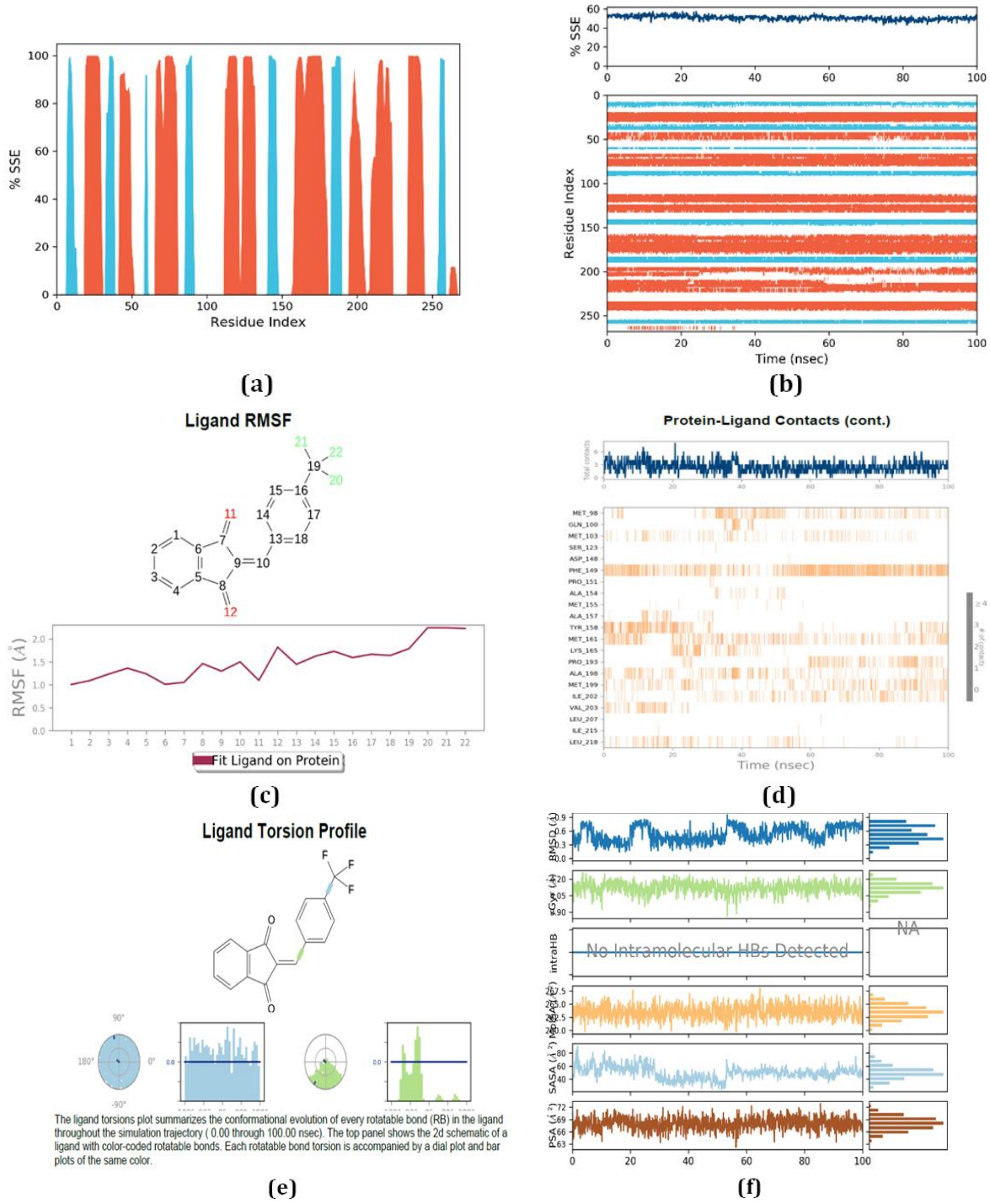

Figure 9. (a) Comparison of the SSE of the 2x23-protein and Compound 11 in MD simulation (a) The 11 residue index and SSE along Y-axis shows differences at the 60–65ns MD simulations period; (b) 2x23-protein shows a little variation at 40–55ns(c) Compound 11 Root-Mean-Square Fluctuation (RMSF) and its interaction with the 2x23 protein are depicted.(d) A timeline showing the total contacts between Compound 11 and the 2x23-protein complex.(e) Torsion profile of Compound 11(f) Various ligand properties including RMSD (Root-Mean-Square Deviation), MolSA (Molecular Surface Area), SASA (Solvent Accessible Surface Area), PSA (Polar Surface Area), rGyr (Radius of Gyration), and intraHB (Intramolecular Hydrogen Bonds) are presented to characterize the ligand.

18.3. Ultimately, it reaches a value of 18.5 after 100 nanoseconds of simulation time (see Figure 8(e)). When the gyration (Rg) decreases, it indicates that the protein is highly orientated when it is attached to a ligand.

The secondary structural elements (SSE) of a protein can change when an inhibitor binds to it. The distribution of protein secondary structural elements (SSE) such as α-helices and β-strands across the protein structure is shown in the graph. In addition, it shows how SSE is composed for every trajectory frame during the course of the simulation. Every residue has been identified, and its secondary structural element has been assigned. Compound 11 behaved consistently over a length of 100 nanoseconds, as seen in Figure 9(a).

There is little effect of 11 and 2x23 interaction on its secondary structure. Moreover, Figure 9(b)'s lower panel illustrates how each amino acid residue contributed to the secondary structural element (SSE) formation of 2x23 throughout the simulation.

The findings of the molecular docking were corroborated by the examination of the intermolecular interactions of the 2x23-protein-11 complex during the MD simulation, as shown in Figure 9(d). The studied trajectories had a 2 is the minimum and 6 is the highest.

Contacts. According to the simulation, the 2x23-protein-11 complex exhibited an average of 6 contacts and a variable number of interactions, ranging from 2 to 9 (Figure 9(d), top panel). Furthermore, during the simulation period, the simulation showed that certain amino acid residues, such as Tyr158, Phe149, Met161, Ala198, Met103, Ile202, and Met161, regularly made contact with 11, as depicted in Figure 9(d)'s lower panel.

The conformational changes that occur in each rotatable bond (RB) in the ligand throughout the course of the simulation (0.00 to 100.00 nsec) are depicted in the ligand torsions figure. A two-dimensional schematic representation of a ligand is shown in the top panel, where rotatable bonds are indicated by distinct color codes. The rotation of bond torsion inside the ligand and protein molecules is shown by the dial plots and bar plots, which share the same colours (Figure 9(e) for Compound 11 and Figure 9(e) for TCU).

The compound had a high molecular surface area (MolSA) of 260 to 267 Å^2, a high polar surface area (PSA) of 66 to 69 Å^2, and a large solvent-accessible surface area (SASA) ranging from 40 to 80 Å^2. As seen in Figure 9(f), these properties helped to keep the compound stable for the course of a 100 ns molecular dynamics (MD) simulation.

Visualizing Radial (or Dial) graphs allows one to study the torsion's conformation during the simulation. The radial map, which displays the temporal evolution of each rotatable bond along the simulation track, has the simulation visible at its center. We may compress the data into bar graphs on the dial plots by depicting the probability density of the torsion. Along with showing the potential of related torsions, the graphic also shows the rotatable bond's capacity based on data from the torsional potential. The potential is plotted on the chart's left Y-axis and is calculated in units of kilocalories per mole (kcal/mol). The conformational strain that the ligand must endure to maintain its shape when bound to a protein may be better understood by examining the histogram and torsion potential.

Conclusion

The fifteen (15) designed derivatives of substituted Indane-1, 3-dione were screened for their docking interaction study, drug likeness using Lipinski's rule of five, pharmacokinetic as well as dynamic simulation study. Based on binding free energy value, hydrogen bonding, and hydrophobic interaction best ligand conformation is chosen. After the compounds under inquiry were evaluated for in silico ADMET prediction, an acceptable ADMET profile

was found including obeying Lipinski's rule of five, skin permeation and molar refractivity lies within the limit of tolerance. Moreover, all designed compounds shows higher GI absorption. All derivatives inhibits isoforms of CYP450 enzyme systems includes inhibitors of CYP-3A4,CYP-2D6,CYP promiscuity shows range from 0.5-0.9.Compounds 1, 4, 9, 11, and 15 had the greatest docking scores when interacting with protein M. tuberculosis InhA (PDB ID: 2x23), according to the findings of the molecular docking studies. Compound 11 poses the highest docking score of -10.38 kcal/mol and shows excellent hydrophobic interactions with amino acid residues such as ILE202, MET98, MET103, PHE97, VAL203, MET199, LEU218, TYR158, MET161, LEU63, PHE149, ILE122, SER94, ILE15, ILE16, ASP148, GLY192, ALA191, MET147, LEU197, and PRO193. The molecular dynamics (MD) simulation analysis showing complex of M. tuberculosis InhA–Compound 11 found to be stable over the simulation period of 100 ns. This implies that Compound 11, 2-[(trifluoromethyl)phenyl]methylidene-1*H*-indene-1,3(2*H*)-dione may have a high binding affinity and be a robust inhibitor of M. tuberculosis InhA. Therefore, it could be a good option for further pharmacological research projects aimed at curing TB.

Acknowledgments

In successfully completing this article and the research behind it, the corresponding author is grateful to all the authors for their helpful contributions.

Disclosure Statement

The authors declare that there is no conflict of interest in this article.

Orcid

Nitin Arjun Londhe: 0009-0004-1936-934X

Karthickeyan Krishnan: 0000-0002-1709-730X

References

[1] K. Mehta, P. Sharma, S. Mujawar, A. Vyas, Role of antimicrobial peptides in treatment and prevention of Mycobacterium tuberculosis: A review, *International Journal of Peptide Research and Therapeutics*, **2022**, *28*, 132. [Crossref], [Google Scholar], [Publisher]

[2] A. Wang, N. Du, H. Song, Y. Zhang, X. Zhong, J. Wu, T. Xue, M. Liu, B. Wang, K. Lv, Design, synthesis and antitubercular activity of novel *N*-(amino) piperazinyl benzothiazinones with improved safety, *European Journal of Medicinal Chemistry*, **2023**, *258*, 115545. [Crossref], [Google Scholar], [Publisher]

[3] M. Pai, T. Kasaeva, S. Swaminathan, Covid-19's devastating effect on tuberculosis care-a path to recovery, *New England Journal of Medicine*, **2022**, *386*, 1490-1493. [Crossref], [Google Scholar], [Publisher]

[4] T.A. Jhaveri, C. Fung, A.N. LaHood, A. Lindeborg, C. Zeng, R. Rahman, P.A. Bain, G.E. Velásquez, C.D. Mitnick, Clinical outcomes of individuals with COVID-19 and tuberculosis during the pre-vaccination period of the pandemic: A systematic review, *Journal of Clinical Medicine*, **2022**, *11*, 5656. [Crossref], [Google Scholar], [Publisher]

[5] W.H.O. *World Tuberculosis Report 2023*; World Health Organization: Geneva, Switzerland, 2023. [Google Scholar]

[6] T.M. Daniel, The history of tuberculosis, *Respiratory Medicine*, **2006**, *100*, 1862-1870. [Crossref], [Google Scholar], [Publisher]

[7] B. Şahin, G. İlgün, Risk factors of deaths related to cardiovascular diseases in World Health Organization (WHO) member countries, *Health & Social Care in the Community*, **2022**, *30*, 73-80. [Crossref], [Google Scholar], [Publisher]

[8] G. Van Den Berg, W.T. Nauta, Effects of anti-inflammatory 2-aryl-1, 3-indandiones on oxidative phosphorylation in rat liver mitochondria, *Biochemical Pharmacology*, **1975**, *24*, 815-821. [Google Scholar]

[9] D. Menzies, Canadian Tuberculosis Standards 8th edition: What's new? And what's next?, *Taylor & Francis*, **2022**, 333-336. [Crossref], [Google Scholar], [Publisher]

[10] D. Falzon, M. Zignol, M. Bastard, K. Floyd, T. Kasaeva, The impact of the COVID-19 pandemic on the global tuberculosis epidemic, *Frontiers in Immunology*, **2023**, *14*, 1234785. [Crossref], [Google Scholar], [Publisher]

[11] J.C. Emery, A.S. Richards, K.D. Dale, C.F. McQuaid, R.G. White, J.T. Denholm, R.M. Houben, Self-clearance of Mycobacterium tuberculosis infection: implications for lifetime risk and population at-risk of tuberculosis disease, *Proceedings of the Royal Society B*, **2021**, *288*, 20201635. [Crossref], [Google Scholar], [Publisher]

[12] H.I. Boshoff, D.F. Warner, B. Gold, Drug-resistant Mycobacterium tuberculosis, *Frontiers in Cellular and Infection Microbiology*, **2023**, *13*, 1215294. [Crossref], [Google Scholar], [Publisher]

[13] D. Vishwakarma, A. Gaidhane, S. Sahu, A.S. Rathod, Multi-drug resistance tuberculosis (MDR-TB) challenges in India: A review, *Cureus*, **2023**, *15*. [Crossref], [Google Scholar], [Publisher]

[14] M.A. Behr, P.H. Edelstein, L. Ramakrishnan, Is Mycobacterium tuberculosis infection life long?, *Bmj*, **2019**, *367*. [Crossref], [Google Scholar], [Publisher]

[15] H.S. Cox, M. Morrow, P.W. Deutschmann, Long term efficacy of DOTS regimens for tuberculosis: Systematic review, *Bmj*, **2008**, *336*, 484-487. [Crossref], [Google Scholar], [Publisher]

[16] W.H. Organization, S.T. Initiative, Treatment of tuberculosis: guidelines, *World Health Organization*, **2010**. [Google Scholar], [Publisher]

[17] M.V.N.d. Souza, T.R.A. Vasconcelos, Fármacos no combate à tuberculose: passado, presente e futuro, *Química Nova*, **2005**, *28*, 678-682. [Google Scholar]

[18] World Health Organization. *Global tuberculosis report 2018*, Genève, Switzerland: World Health Organization, **2018**.

[19] J.I. Silesky-Jiménez, Tuberculosis Multidrug Resistance (MDR-TB), *Highly Infectious Diseases in Critical Care: A Comprehensive Clinical Guide*, **2020**, 235-252. [Crossref], [Google Scholar], [Publisher]

[20] M. Daffé, P. Draper, The envelope layers of mycobacteria with reference to their pathogenicity, *Advances in Microbial Physiology*, **1997**, *39*, 131-203. [Crossref], [Google Scholar], [Publisher]

[21] J. Pawełczyk, L. Kremer, The molecular genetics of mycolic acid biosynthesis, *Molecular Genetics of Mycobacteria*, **2014**, 611-631. [Crossref], [Google Scholar], [Publisher]

[22] P.S. Phatak, R.D. Bakale, S.T. Dhumal, L.K. Dahiwade, P.B. Choudhari, V. Siva Krishna, D. Sriram, K.P. Haval, Synthesis, antitubercular evaluation and molecular docking studies of phthalimide bearing 1, 2, 3-triazoles, *Synthetic Communications*, **2019**, *49*, 2017-2028. [Crossref], [Google Scholar], [Publisher]

[23] S.R. Luckner, N. Liu, C.W. Am Ende, P.J. Tonge, C. Kisker, A slow, tight binding inhibitor of InhA, the enoyl-acyl carrier protein reductase from Mycobacterium tuberculosis, *Journal of Biological Chemistry*, **2010**, *285*, 14330-14337. [Crossref], [Google Scholar], [Publisher]

[24] S. Thapa, M.S. Biradar, S.L. Nargund, I. Ahmad, M. Agrawal, H. Patel, A. Lamsal, Synthesis, molecular docking, molecular dynamic simulation studies, and antitubercular activity evaluation of substituted benzimidazole derivatives,

Advances in Pharmacological and Pharmaceutical Sciences, **2024**, *2024*. [Crossref], [Google Scholar], [Publisher]

[25] S.S. Rani, Shivaraj, Subhashini, Design, synthesis and pharmacological evaluation of novel 1,3-indanedione derivatives, *Indo American Journal of Pharmaceutical Sciences*, **2018**, *5*, 1969-1979. [Crossref], [Google Scholar]

[26] T. Nishiyama, S. Shiotsu, H. Tsujita, Antioxidative activity and active site of 1, 3-indandiones with the *β*-diketone moiety, *Polymer Degradation and Stability*, **2002**, *76*, 435-439. [Crossref], [Google Scholar], [Publisher]

[27] G. Van Den Berg, W.T. Nauta, Effects of anti-inflammatory 2-aryl-1, 3-indandiones on oxidative phosphorylation in rat liver mitochondria, *Biochemical Pharmacology*, **1975**, *24*, 815-821. [Crossref], [Google Scholar], [Publisher]

[28] R.M. Houben, P.J. Dodd, The global burden of latent tuberculosis infection: A re-estimation using mathematical modelling, *PLoS Medicine*, **2016**, *13*, e1002152. [Crossref], [Google Scholar], [Publisher]

[29] F. Chen, L. Liu, Z. Bai, T. Zhang, K. Zhao, Synthesis and biological activity of the novel indanedione anticoagulant rodenticides containing fluorine, *Bioengineered*, **2017**, *8*, 92-98. [Crossref], [Google Scholar], [Publisher]

[30] V.V. Dhayabaran, T.D. Prakash, R. Renganathan, E. Friehs, D.W. Bahnemann, Novel Bioactive Co (II), Cu (II), Ni (II) and Zn (II) Complexes with Schiff base ligand derived from histidine and 1, 3-Indandione: Synthesis, structural elucidation, biological investigation and Docking analysis, *Journal of fluorescence*, **2017**, *27*, 135-150. [Crossref], [Google Scholar], [Publisher]

[31] C.B. Mishra, A. Manral, S. Kumari, V. Saini, M. Tiwari, Design, synthesis and evaluation of novel indandione derivatives as multifunctional agents with cholinesterase inhibition, anti-*β*-amyloid aggregation, antioxidant and neuroprotection properties against Alzheimer's disease, *Bioorganic & Medicinal Chemistry*, **2016**, *24*, 3829-3841. [Crossref], [Google Scholar], [Publisher]

[32] B. Bano, K.M. Khan, F. Begum, M.A. Lodhi, U. Salar, R. Khalil, Z. Ul-Haq, S. Perveen, Benzylidine indane-1, 3-diones: As novel urease inhibitors; synthesis, in vitro, and in silico studies, *Bioorganic Chemistry*, **2018**, *81*, 658-671. [Crossref], [Google Scholar], [Publisher]

[33] C.G. Thomson, K. Duncan, S.R. Fletcher, I.T. Huscroft, G. Pillai, P. Raubo, A.J. Smith, D. Stead, Sarcosine based indandione hGlyT1 inhibitors, *Bioorganic & Medicinal Chemistry Letters*, **2006**, *16*, 1388-1391. [Crossref], [Google Scholar], [Publisher]

[34] F. Köhler, K. Fickentscher, U. Halfmann, H. Koch, Embryotoxicity and teratogenicity of derivatives of 1, 3-indandion, *Archives of Toxicology*, **1975**, *33*, 191-197. [Crossref], [Google Scholar], [Publisher]

[35] D.R. Buckle, N.J. Morgan, J.W. Ross, H. Smith, B.A. Spicer, Antiallergic activity of 2-nitroindan-1, 3-diones, *Journal of Medicinal Chemistry*, **1973**, *16*, 1334-1339. [Crossref], [Google Scholar], [Publisher]

[36] M. Jeyachandran, P. Ramesh, Synthesis, antimicrobial, and anticoagulant activities of 2-(arylsulfonyl) indane-1,3-diones, *Organic Chemistry International*, **2011**, *2011*. [Crossref], [Google Scholar], [Publisher]

[37] S.L. Shapiro, K. Geiger, L. Freedman, Indandione anticoagulants, *The Journal of Organic Chemistry*, **1960**, *25*, 1860-1865. [Crossref], [Google Scholar], [Publisher]

[38] K. Raval, T. Ganatra, Basics, types and applications of molecular docking: A review, *IP International Journal of Comprehensive and Advanced Pharmacology*, **2022**, *7*, 12-16. [Crossref], [Google Scholar], [Publisher]

[39] S. Tiwari, K. Prakash, Unrevealing the complex interplay: Molecular docking: a comprehensive review on current scenario, upcoming difficulties, forthcoming initiatives, and viewpoints, *International Journal of Chemistry Research*, **2024**, 1-9. [Crossref], [Google Scholar], [Publisher]

[40] S.A.A. Anand, C. Loganathan, K. Saravanan, S. Kabilan, Comparison of molecular docking and molecular dynamics simulations of 1, 3-thiazin-4-one with MDM2 protein, *International Letters of Chemistry, Physics and Astronomy*, **2015**, *60*, 161-167. [Google Scholar]

[41] L. Orellana, Large-scale conformational changes and protein function: Breaking the in silico barrier, *Frontiers in Molecular Biosciences*, **2019**, *6*, 117. [Crossref], [Google Scholar], [Publisher]

[42] H. Geng, F. Chen, J. Ye, F. Jiang, Applications of molecular dynamics simulation in structure prediction of peptides and proteins, *Computational and Structural Biotechnology Journal*, **2019**, *17*, 1162-1170. [Crossref], [Google Scholar], [Publisher]

[43] L.M. Mihalovits, G.G. Ferenczy, G.M. Keserű, Mechanistic and thermodynamic characterization of oxathiazolones as potent and selective covalent immunoproteasome inhibitors, *Computational and Structural Biotechnology Journal*, **2021**, *19*, 4486-4496. [Crossref], [Google Scholar], [Publisher]

[44] D. Lau, W. Jian, Z. Yu, D. Hui, Nano-engineering of construction materials using molecular dynamics simulations: Prospects and challenges, *Composites Part B: Engineering*, **2018**, *143*, 282-291. [Crossref], [Google Scholar], [Publisher]

[45] S.K. Halder, F. Elma, In silico identification of novel chemical compounds with antituberculosis activity for the inhibition of InhA and EthR proteins from Mycobacterium tuberculosis, *Journal of Clinical Tuberculosis and Other Mycobacterial Diseases*, **2021**, *24*, 100246. [Crossref], [Google Scholar], [Publisher]

[46] S. Dallakyan, A.J. Olson, Small-molecule library screening by docking with PyRx, *Chemical Biology: Methods and Protocols*, **2015**, 243-250. [Crossref], [Google Scholar], [Publisher]

[47] T.A. Halgren, Identifying and characterizing binding sites and assessing druggability, *Journal of Chemical Information and Modeling*, **2009**, *49*, 377-389. [Crossref], [Google Scholar], [Publisher]

[48] A.K. Rappé, C.J. Casewit, K. Colwell, W.A. Goddard III, W.M. Skiff, UFF, a full periodic table force field for molecular mechanics and molecular dynamics simulations, *Journal of the American Chemical Society*, **1992**, *114*, 10024-10035. [Crossref], [Google Scholar], [Publisher]

[49] B. Adegoke Afeez, M. Adeleke, A. Habeeb, Statistical analysis of the inhibitory activities of triterpenoid derivatives against two selected diseases, *International Journal of Research, Innovation, and Applied Sciences*, **2019**, *4*, 130–135. [Google Scholar], [Publisher]

[50] G.M. Sastry, M. Adzhigirey, T. Day, R. Annabhimoju, W. Sherman, Protein and ligand preparation: parameters, protocols, and influence on virtual screening enrichments, *Journal of Computer-Aided Molecular Design*, **2013**, *27*, 221-234. [Crossref], [Google Scholar], [Publisher]

[51] A. Mollica, G. Zengin, S. Durdagi, R.E. Salmas, G. Macedonio, A. Stefanucci, M.P. Dimmito, E. Novellino, Combinatorial peptide library screening for discovery of diverse alpha-glucosidase inhibitors using molecular dynamics simulations and binary QSAR models, *Journal of Biomolecular Structure and Dynamics*, **2019**, *37*, 726-740. [Crossref], [Google Scholar], [Publisher]

[52] W.L. Jorgensen, D.S. Maxwell, J. Tirado-Rives, Development and testing of the OPLS all-atom

force field on conformational energetics and properties of organic liquids, *Journal of the American Chemical Society*, **1996**, *118*, 11225-11236. [Crossref], [Google Scholar], [Publisher]

[53] A. Adegoke, T. Oyelowo, J. Sanusi, Computational Studies of 1, 2, 3-Triazoles Derivatives against Yellow Fever Virus: DFT-Based, *European Modern Journal Studies*, **2020**, *4*, 94-103. [Google Scholar]

[54] A.C. Wallace, R.A. Laskowski, J.M. Thornton, LIGPLOT: a program to generate schematic diagrams of protein-ligand interactions, *Protein Engineering, Design and Selection*, **1995**, *8*, 127-134. [Crossref], [Google Scholar], [Publisher]

[55] B. Yazdani, H. Sirous, S. Brogi, V. Calderone, Structure-based high-throughput virtual screening and molecular dynamics simulation for the discovery of novel SARS-CoV-2 NSP3 Mac1 domain inhibitors, *Viruses*, **2023**, *15*, 2291. [Crossref], [Google Scholar], [Publisher]

[56] Y. Yue, S. Zhao, Y. Sun, X. Yan, J. Liu, J. Zhang, Effects of plant extract aurantio-obtusin on pepsin structure: spectroscopic characterization and docking simulation, *Journal of Luminescence*, **2017**, *187*, 333-339. [Crossref], [Google Scholar], [Publisher]

[57] W.L. Jorgensen, J. Chandrasekhar, J.D. Madura, R.W. Impey, M.L. Klein, Comparison of simple potential functions for simulating liquid water, *The Journal of Chemical Physics*, **1983**, *79*, 926-935. [Crossref], [Google Scholar], [Publisher]

[58] W.G. Hoover, Canonical dynamics: Equilibrium phase-space distributions, *Physical review A*, **1985**, *31*, 1695. [Crossref], [Google Scholar], [Publisher]

[59] G.J. Martyna, D.J. Tobias, M.L. Klein, Constant pressure molecular dynamics algorithms, *The Journal of Chemical Physics*, **1994**, *101*, 4177-4189. [Crossref], [Google Scholar], [Publisher]

[60] U. Essmann, L. Perera, M.L. Berkowitz, T. Darden, H. Lee, L.G. Pedersen, A smooth particle mesh Ewald method, *The Journal of Chemical Physics*, **1995**, *103*, 8577-8593. [Crossref], [Google Scholar], [Publisher]

[61] A.B. Adegoke, R.A. Adepoju, A.T.-A. Khan, Molecular Dynamic (MD) Simulation and Modeling the Bio-molecular Structure of Human UDP glucose-6-dehydrogenase Isoform 1 (hUGDH) Related to Prostate Cancer, *Basrah Journal of Science*, **2020**, *38*, 448-466. [Google Scholar]

[62] R. Girase, I. Ahmad, H. Patel, Bioisosteric modification of Linezolid identified the potential M. tuberculosis protein synthesis inhibitors to overcome the myelosuppression and serotonergic toxicity associated with Linezolid in the treatment of the multi-drug resistance tuberculosis (MDR-TB), *Journal of Biomolecular Structure and Dynamics*, **2024**, *42*, 2111-2126. [Crossref], [Google Scholar], [Publisher]

[63] V.R. Jagatap, I. Ahmad, D. Sriram, J. Kumari, D.K. Adu, B.W. Ike, M. Ghai, S.A. Ansari, I.A. Ansari, P.O.M. Wetchoua, Isoflavonoid and furanochromone natural products as potential DNA gyrase inhibitors: Computational, spectral, and antimycobacterial studies, *ACS Omega*, **2023**, *8*, 16228-16240. [Crossref], [Google Scholar], [Publisher]

[64] C.A. Lipinski, Lead-and drug-like compounds: the rule-of-five revolution, *Drug Discovery Today: Technologies*, **2004**, *1*, 337-341. [Crossref], [Google Scholar], [Publisher]

[65] D. Cao, J. Wang, R. Zhou, Y. Li, H. Yu, T. Hou, ADMET evaluation in drug discovery. 11. PharmacoKinetics Knowledge Base (PKKB): a comprehensive database of pharmacokinetic and toxic properties for drugs, *Journal of Chemical Information and Modeling*, **2012**, *52*, 1132-1137. [Crossref], [Google Scholar], [Publisher]

[66] D.E. Pires, T.L. Blundell, D.B. Ascher, pkCSM: predicting small-molecule pharmacokinetic and toxicity properties using graph-based signatures, *Journal of Medicinal Chemistry*,

2015, *58*, 4066-4072. [Crossref], [Google Scholar], [Publisher]

[67] H. Yang, C. Lou, L. Sun, J. Li, Y. Cai, Z. Wang, W. Li, G. Liu, Y. Tang, admetSAR 2.0: web-service for prediction and optimization of chemical ADMET properties, *Bioinformatics*, **2019**, *35*, 1067-1069. [Crossref], [Google Scholar], [Publisher]

[68] A. Adegoke, A.G. Olatunji, L.I. Ajerogba, I. Musa, Theoretical studies of 1, 2, 3-triazole and isoxazole-linked pyrazole hybrids as antibacterial agents: An approach of docking and density functional theory, *Advanced Journal of Chemistry, Section B*, **2020**. [Crossref], [Google Scholar], [Publisher]

[69] J.V. Borba, V.M. Alves, R.C. Braga, D.R. Korn, K. Overdahl, A.C. Silva, S.U. Hall, E. Overdahl, N. Kleinstreuer, J. Strickland, STopTox: An in silico alternative to animal testing for acute systemic and topical toxicity, *Environmental Health Perspectives*, **2022**, *130*, 027012. [Crossref], [Google Scholar], [Publisher]

HOW TO CITE THIS ARTICLE

N.A. Londhe, K. Krishnan. In Depth Computational Screening of Novel Indane-1, 3-Dione Derivatives as Potential Anti-Tubercular Agents. *Adv. J. Chem. A*, 2024, 7(5), 576-606.

DOI: 10.48309/AJCA.2024.453614.1514
URL: https://www.ajchem-a.com/article_197272.html